Published in final edited form as:
J Comp Neurol. 2013 April 15; 521(6): 1225–1250. doi:10.1002/cne.23290.

Distribution and Intrinsic Membrane Properties of Basal Forebrain GABAergic and Parvalbumin Neurons in the Mouse

James T. McKenna[1], **Chun Yang**[1], **Serena Franciosi**[1,2], **Stuart Winston**[1], **Kathleen K. Abarr**[3], **Matthew S. Rigby**[3], **Yuchio Yanagawa**[4], **Robert W. McCarley**[1], and **Ritchie E. Brown**[1,*]

[1]Laboratory of Neuroscience, VA Boston Healthcare System and Harvard Medical School, Department of Psychiatry, Brockton, Massachusetts, 02301

[2]Institute of Human Physiology II, University of Milan Medical School, Milan, Italy

[3]Stonehill College, Easton, Massachusetts, 02357

[4]Department of Genetic and Behavioural Neuroscience, Gunma University Graduate School of Medicine and CREST, JST, Maebashi 371-8511, Japan

Abstract

The basal forebrain (BF) strongly regulates cortical activation, sleep homeostasis, and attention. Many BF neurons involved in these processes are GABAergic, including a subpopulation of projection neurons containing the calcium-binding protein, parvalbumin (PV). However, technical difficulties in identification have prevented a precise mapping of the distribution of GABAergic and GABA/PV+ neurons in the mouse or a determination of their intrinsic membrane properties. Here we used mice expressing fluorescent proteins in GABAergic (GAD67-GFP knock-in mice) or PV+ neurons (PV-Tomato mice) to study these neurons. Immunohistochemical staining for GABA in GAD67-GFP mice confirmed that GFP selectively labeled BF GABAergic neurons. GFP+ neurons and fibers were distributed throughout the BF, with the highest density in the magnocellular preoptic area (MCPO). Immunohistochemistry for PV indicated that the majority of PV+ neurons in the BF were large (>20 μm) or medium-sized (15–20 μm) GFP+ neurons. Most medium and large-sized BF GFP+ neurons, including those retrogradely labeled from the neocortex, were fast-firing and spontaneously active in vitro. They exhibited prominent hyperpolarization-activated inward currents and subthreshold “spikelets,” suggestive of electrical coupling. PV+ neurons recorded in PV-Tomato mice had similar properties but had significantly narrower action potentials and a higher maximal firing frequency. Another population of smaller GFP+ neurons had properties similar to striatal projection neurons. The fast firing and electrical coupling of BF GABA/PV+ neurons, together with their projections to cortical interneurons and the thalamic reticular nucleus, suggest a strong and synchronous control of the neocortical fast rhythms typical of wakefulness and REM sleep.

*Correspondence to: Ritchie E. Brown, Ph.D., In Vitro Neurophysiology Laboratory, Department of Psychiatry, VA Boston Healthcare System and Harvard Medical School, VA Medical Center Brockton, Research 151C, 940 Belmont St., Brockton, MA, 02301. Ritchie_Brown@hms.harvard.edu.

Additional Supporting Information may be found in the online version of this article.

Conflict of Interest: No conflicts of interest have been identified for any of the authors.

Role of Authors: All authors had access to all the data in the study and took responsibility for the integrity of the data and the accuracy of the data analysis. Study concept and design: JTM, CY, RWM, REB. Acquisition of data: JTM, CY, SF, SW, KA, MR, REB. Analysis and interpretation of data: JTM, CY, SF, KA, MR, REB. Drafting of the article JTM, CY, REB. Critical revision of the article for important intellectual content: JTM, CY, YY, RWM, REB. Statistical Analysis: JTM, CY, SF. Obtained funding: YY, RWM, REB. Material Support: YY. Study supervision: RWM, REB.

Indexing Terms

green fluorescent protein; glutamic acid decarboxylase; electrical coupling; H-current; parvalbumin

The basal forebrain (BF) is important for processes of cortical activation (Detari et al., 1999), sleep homeostasis (Strecker et al., 2000), and attention (Burk and Sarter, 2001; Lin and Nicolelis, 2008). Neurotoxic lesions (Buzsaki et al., 1988; Kaur et al., 2008; Fuller et al., 2011) or pharmacological inactivation of the BF (Cape and Jones, 2000) decrease neocortical fast activity typical of wakefulness and REM sleep, cause deficits in attention (Burk and Sarter, 2001), and prevent the rebound of sleep observed after sleep deprivation (Kalinchuk et al., 2008; Kaur et al., 2008), underscoring its importance in the control of behavioral state.

An understanding of how the BF functions requires the ability to study the properties of its component neurons, identified according to their neurotransmitter phenotype. While BF cholinergic neurons have been the topic of many studies (Jones, 2004), less is known about the large population of BF GABAergic neurons due to technical difficulties in identification. For instance, a detailed analysis of the distribution, morphology, and size of BF GABAergic neurons has not been reported in the mouse, a species increasingly used for neurophysiological and behavioral studies due to the availability of genetically modified animals.

Different subpopulations of BF GABAergic neurons are involved in cortical activation and sleep (Hassani et al., 2009). One subpopulation of particular interest contains the calcium-binding protein parvalbumin (PV). In the rat, these neurons are medium or large-sized GABAergic neurons (Gritti et al., 2003), which project to cortical interneurons containing PV or somatostatin (Freund and Meskenaite, 1992; Henny and Jones, 2008) and to the thalamic reticular nucleus (Jourdain et al., 1989; Bickford et al., 1994). This projection pattern is especially interesting since both cortical PV+ interneurons (Sohal et al., 2009; Cardin et al., 2009) and PV+ thalamic reticular nucleus neurons (Pinault and Deschenes, 1992) are important in generating fast electroencephalographic (EEG) rhythms in the gamma (30–80 Hz) range associated with attentional processing (Gregoriou et al., 2009; Tiesinga and Sejnowski, 2009).

Consistent with a role in control of cortical fast rhythms, studies of the state-dependent firing of BF GABAergic (Manns et al., 2000; Hassani et al., 2009) or PV+ neurons (Duque et al., 2000) using juxtacellular recording methods and post-hoc labeling identified a population of large neurons which fired rhythmically at beta/gamma frequencies (20–60 Hz) in association with cortical activation. Furthermore, in preliminary experiments optogenetic stimulation of BF PV+ neurons entrained cortical gamma rhythms (Kim et al., 2011). However, how the fast rhythmic firing pattern of these neurons is generated is unclear, due to the inability to identify and study the properties of BF GABAergic or PV+ neurons in vitro.

Here we validated the use of mice expressing fluorescent proteins in GABAergic (GAD67-GFP knock-in mice) (Tamamaki et al., 2003) and PV neurons (PV-Tomato mice) to study BF GABAergic and PV+ neurons. We mapped their location and determined the extent of their colocalization. In addition, we provide the first in vitro characterization of the intrinsic membrane properties of identified BF GABAergic and PV+ neurons. Parts of these results have been presented in abstract form (Brown et al., 2007, 2008a; McKenna et al., 2010, 2011).

Materials and Methods

Animals

In order to identify BF GABAergic neurons, we used heterozygous GAD67-GFP knock-in mice (Tamamaki et al., 2003; Brown et al., 2008b). Male, heterozygous GAD67-GFP mice (RIKEN Bioresource Center, http://www.brc.riken.jp/lab/animal/en, strain RBRC03674) on a Swiss-Webster background were crossed with female wildtype Swiss-Webster mice to generate the animals used in this study. Although heterozygous animals lack one copy of the GAD67 gene, the sleep-wake behavior and cortical activation of these animals is indistinguishable from that of wildtype animals (Chen et al., 2010). Both male and female animals were used for neuroanatomical and electrophysiological investigations. In order to identify PV containing neurons we crossed PV-Cre mice (Strain 008069; Jackson Labs, Bar Harbor, ME) with a Cre-reporter strain (Strain 007905; Jackson Labs) resulting in mice expressing red (Tomato) fluorescence in neurons expressing PV (PV-Tomato mice).

For immunohistochemical staining and mapping experiments, we used adult animals to facilitate the transcardial perfusion of fixative. Since the extensive myelination in the BF after postnatal age P21 impairs infrared visualization of the neurons, for most in vitro electrophysiological recordings we used juvenile (12–21-day) animals. As expected, the number, morphology, and distribution of fluorescent neurons in GAD67-GFP mice was similar when comparing adult mice used for immunohistochemistry and younger animals used for electrophysiology, since GFP expression driven by the GAD67 promoter begins prenatally (Tamamaki et al., 2003). In addition, we confirmed our in vitro electrophysiology results in recordings from a smaller cohort of adult animals. In PV-Tomato mice, fluorescent neurons were observed at postnatal 14 but not earlier, consistent with the later expression of the PV gene (Seto-Ohshima et al., 1990; Solbach and Celio, 1991).

Mice were housed under constant temperature and a 12:12 hr light:dark cycle (7AM:7PM), with food and water available ad libitum. All experiments conformed to U.S. Veterans Administration, Harvard University, and U.S. National Institutes of Health guidelines on the ethical use of animals. All measures were taken to minimize the number of animals used and their suffering, and were carried out in accordance with the National Institutes of Health *Guide for the Care and Use of Laboratory Animals* (NIH Publications No. 80-23). Experimental procedures were approved by the Institutional Animal Care and Use Committee of the VA Boston Healthcare System.

Target area within the BF

For both immunohistochemical staining and electrophysiological experiments we focused on intermediate areas of the basal forebrain (substantia innominata [SI], horizontal limb of the diagonal band [HDB], magnocellular preoptic nucleus [MCPO] and ventral pallidum [VP]) where previous studies in the rat (Rye et al., 1984; Gritti et al., 2003; Henny and Jones, 2008) have found neurons projecting to the neocortex. Our analysis did not include the rostral aspect of BF (medial septum, vertical limb of the diagonal band [MS/DBV]), a portion of which contains neurons projecting to the hippocampus, or the caudal magnocellular basal nucleus, although GFP+ neurons were also located in these areas. Therefore, our investigations were largely of intermediate levels of the basal forebrain.

Immunohistochemistry

Immunohistochemical colocalization of GFP and GABA—To confirm the validity of the GAD67-GFP mouse model (i.e., if GFP labels all BF GABAergic neurons), we performed immunohistochemistry for GABA. Consistent with previous studies in the BF (Panula et al., 1984; Onteniente et al., 1986; Gritti et al., 1998, 2003) preliminary

experiments determined that GABA immunohistochemis-try only labeled a small percentage of BF neurons, likely due to the low levels of antigens in cell bodies and/or poor antibody penetration. Therefore, to enhance the level of GABA we used an inhibitor of axonal transport, colchicine, to enhance detection. Heterozygous GAD67-GFP knock-in mice (n = 4), weighing ~30 g, were deeply anesthetized by inhalation of 3% isoflurane. Mice were then bilaterally injected with 0.1 μl of a colchicine solution (10 μg in 1 μl phosphate-buffered saline [PBS, pH = 7.4] per injection site) into BF (−0.10 mm AP, ±1.5 mm ML, −5.4 DV, relative to Bregma; Fig. 1A) using a 1-μl Hamilton microsyringe (Sigma Aldrich, St. Louis, MO; Model 80100, Cat. no. 20731: needle size 25G, blunt tip). The health of the animals was closely monitored following the colchicine injections, and no distress was observed. After a survival time of 1–2 days, mice were sacrificed, brains extracted, and immunohistochemistry performed for GABA (see next section).

Immunohistochemistry methods

Gaba: Coronal sections from GAD67-GFP knock-in mice containing BF from one collected well (see General Methods section below for perfusion/fixation and sectioning techniques) were first washed with PBS (pH = 7.4), and then blocked and incubated overnight at room temperature (RT) with rabbit anti-GABA primary antibody (1:200; A2052; Sigma). On the following day, slices were incubated for 3.5 hours at RT in donkey anti-rabbit IgG secondary antibody conjugated to AlexaFluor 594 (red; 1:100; A21207; Invitrogen, La Jolla, CA).

Choline acetyl-transferase (ChAT): To determine if GFP was located ectopically in BF cholinergic neurons in GAD67-GFP knock-in mice, coronal slices from one well were washed with PBS, placed in a blocking solution, and then incubated in rabbit anti-ChAT (the synthetic enzyme for acetylcholine) for two nights at 4°C (1:200; AB143; Millipore, Bedford, MA). After incubation, tissue was rinsed and treated for 3 hours at RT in secondary antibody, donkey anti-rabbit IgG conjugated with AlexaFluor 594 (red; 1:100; A21207; Invitrogen).

Parvalbumin (PV): For localization of PV+ and GABA/PV+ neurons in BF, slices containing BF from another well collected from GAD67-GFP mice were washed with PBS, placed in a blocking solution, and then incubated in rabbit anti-PV for two nights at 4°C (1:200; AB11427; Abcam, Cambridge, MA). Tissue was then rinsed, and incubated for 4 hours at RT in secondary antibody, donkey anti-rabbit IgG conjugated to AlexaFluor 594 (red; 1:100; A21207; Invitrogen).

PV staining was confirmed with a primary mouse-anti PV antibody. Since this antibody is produced in the mouse, we used the M.O.M. detection kit (Cat. no. FMK-2201; Vector Laboratories, Burlingame, CA), which blocked the endogenous activity of mouse immunoglobulins, allowing localization of mouse primary antibodies on mouse tissue. Sections were labeled with mouse anti-PV (1:200; Cat. no. MAB1572; Millipore) and secondary rabbit anti-mouse IgG conjugated to AlexaFluor 594 (red; 1:300; A11062; Invitrogen).

To confirm that Tomato red fluorescence is a selective marker for PV neurons in PV-Tomato mice, we immunohistochemically labeled BF slices from these mice for PV. Coronal slices from one well were blocked and incubated in rabbit anti-PV for 2 nights at 4°C (1:200; AB11427; Abcam). On the following day, slices were incubated for 3.5 hours at RT in donkey anti-rabbit IgG secondary antibody conjugated to AlexaFluor 488 (green; 1:100; A21206; Invitrogen).

Antibody characterization—All primary antibodies employed here have been previously used and validated in peer-reviewed publications (Table 1). Secondary antibody-only controls were also performed for all four immunolabeling procedures, omitting the primary antibodies.

Gaba: The polyclonal anti-gamma aminobutyric acid antibody (anti-GABA, 1:200; A2052; Sigma; Antibody Registry [Neuroscience Information Framework] no. AB_477652; http://antibodyregistry.org/AB_477652) was raised in rabbits against synthetic GABA conjugates to bovine albumin serum (BSA), and binds to GABA but not BSA (dot blot assays, manufacturer's data). This antibody has been previously characterized (e.g., Stillman et al., 2009; Suzuki and Beckers, 2010; Xu et al., 2010). GABA immunoreactivity was observed in many brain regions, similar to previously reported GABA/GAD67 immunostaining results in the mouse (Ottersen and Storm-Mathisen, 1984; Smith et al., 1994; Brown et al., 2008b; Kim et al., 2012) and rat (Spreafico et al., 1991; Gritti et al., 1994, 1997; Brischoux et al., 2008), including the cortex, pre-optic regions, BF, reticular nucleus of the thalamus, and numerous brainstem regions.

Choline acetyl-transferase (ChAT): The polyclonal anti-choline acetyltransferase antibody (anti-ChAT, 1:200; AB143; Millipore; Antibody Registry no. AB_90637; http://antibodyregistry.org/AB_90637) was raised in rabbits, and precipitated a 68 kDa band on western blots from human placental and brain cells (immunogen of human placental ChAT, manufacturer's data). This antibody has been previously characterized (e.g., Hassani et al., 2009; Stillman et al., 2009; Martin-Ibanez et al., 2010). Regions expressing ChAT immunoreactivity were similar to those previously reported employing different anti-ChAT antibodies in the mouse (Levey et al., 1983; Kalogiannis et al., 2010; Unal et al., 2012) and rat (Rye et al., 1984, 1987; Semba and Fibiger, 1992; Gritti et al., 1993), including the medial septum/ventral nucleus of the diagonal band (MS/DBV), BF subnuclei as investigated here, striatum, and the pontine tegmental region.

Parvalbumin (PV): The polyclonal anti-parvalbumin antibody (anti-PV; AB11427; Abcam, 1:200; Antibody Registry no. AB_298032; http://antibodyregistry.org/AB_298032) was raised in rabbits against rat muscle PV antigen and precipitated a single 12 kDa band on western blots from rat cerebellum (manufacturer's data). This antibody has been previously characterized (e.g., Bowser and Khakh, 2004; Akgul and Wollmuth, 2010; McCurry et al., 2010). We also employed another monoclonal anti-PV antibody to confirm labeling (MAB1572, 1:200; Millipore; Antibody Registry no. AB_94262; http://antibodyregistry.org/AB_94262), which was raised in mouse against frog muscle PV antigen. This antibody precipitated a 12-kDa band on western blots from rat brain lysates (manufacturer's data). This antibody has also been previously characterized (e.g., Perrotti et al., 2004; Peng and Howser, 2005; Siembab et al., 2010). PV staining employing either antibody labeled neurons throughout many brain regions, similar to that previously reported using different antibodies in the mouse (Xu et al., 2006; Chang et al., 2007; Kim et al., 2012) and rat (Endo et al., 1986; Duque et al., 2000; Gritti et al., 2003; Deurveilher et al., 2006), including the cortex, BF, and the reticular nucleus of the thalamus.

General immunohistochemistry methods—Mice were deeply anesthetized with sodium pentobarbital (50 mg/ml), exsanguinated with saline, and perfused transcardially with a solution of 10% buffered formalin and 0.1% glutaraldehyde. Brains were postfixed for 4 hours, then transferred to a 30% sucrose solution for 48 hours at 4°C. Tissue was cut at a thickness of 40 μm on a freezing microtome and collected into four wells of PBS.

Following all immunohistochemistry procedures, tissue was washed and mounted onto chrome-alum gelatin-coated slides, dried, and coverslipped using Vectashield hard set

mounting medium (H-1400; Vector Laboratories). Staining and quantification for each neuronal marker was conducted in four animals. For each immunolabeling stain (ChAT, GABA, PV), we quantified three representative coronal section levels per animal (0.38 mm [rostral], .014 mm [medial], and −0.10 mm [caudal] from Bregma), which roughly spanned the rostrocaudal extent of BF regions projecting to the neocortex (~0.6 mm) using Neurolucida software (v.8; MicroBrightField, Williston, VT) and an Olympus BX51 microscope. These slices corresponded approximately to the midpoints of the three slices used for electrophysiological recordings (see below).

Cellular mapping and photography—The perimeter and landmarks of BF and the four subnuclei were first traced at a low magnification (10×), and neuronal location was then plotted at higher magnification (20–40×) and imposed on the Neurolucida sketches of brain areas and landmarks generated at 10× magnification. The distribution of labeled neurons was determined using a mouse brain atlas (Franklin and Paxinos, 2008). Measures (counts and long-axis diameter measures) were then determined within the different subnuclei. We employed the Franklin and Paxinos templates (2008), and mapped the representative case that best matched the template subnuclei boundaries (Fig. 3). Once tracing and cell plotting was completed in Neurolucida, this sketch was placed on top of the Adobe Illustrator templates (employing the “Transparency” tool). Symbols were then replotted in Adobe Illustrator (CS5, v. 15.1.0, San Jose, CA) superimposed on the cell mapping originally done in Neurolucida.

GFP+ neurons were identified by the presence of green fluorescence in the cytoplasm and nucleus (excitation:emission 488:509 nm). GABAergic, ChAT+, and PV+ cells were identified by the presence of red (excitation/emission at 590:617 nm) fluorescence in the cytoplasm and nucleus. In PV-Tomato mice where a red fluorescent protein (Tomato) is expressed under the control of the PV promoter we confirmed selective expression using a PV antibody and a secondary antibody tagged with a green fluorophore (excitation:emission 488:509 nm). GFP+ neurons were determined to be colocalized with GABA, ChAT, or PV if yellow/orange soma was observed (overlay of green and red fluorescence). The long-axis diameter of labeled neurons was measured for each of the four BF subnuclei using Neurolucida software. Ten neurons were randomly selected from photomicrographs taken within each subnuclei (20× magnification), and measured/analyzed bilaterally, for the three representative slices (rostral, medial, and caudal) in each animal ($n = 4$). Digital images of fluorescently labeled neurons were captured using a deconvolution Zeiss Axio-plan 2 microscope and Slidebook system (3i Intelligent Imaging Innovations; Denver, CO). Image clarity was enhanced by adjusting the contrast and brightness in the Slidebook and/or Adobe Photoshop image processing software. Figures that include multiple panels were assembled using Adobe Photoshop (CS5, v. 12.1 ×64), except for cellular mapping (Fig. 3), where they were assembled using Adobe Illustrator (CS5, v. 15.1.0).

Statistical analysis (neuroanatomy)—All neuroanatomical density, long-axis diameter, and colocalization measures were analyzed using two-way analysis of variance (ANOVA), where one independent variable was the subnucleus of BF (VP, SI, HDB, MCPO), and the second independent variable was the three coronal BF slice representations (rostral, medial, and caudal). If measures were found to significantly differ, a pair-wise independent t-test comparison between groups was then made, using Bonferroni correction. Statistical analysis utilized SPSS software (release 11.5, Chicago, IL), and differences determined to be significant when $P < 0.05$.

Electrophysiology

Preparation of BF slices for electrophysiological recordings—Young (12-21 days) mice were deeply anesthetized with isoflurane and then decapitated. 250- or 300-μm thick, coronal BF slices were cut between 0.50 mm and −0.22 mm with respect to Bregma rostrocaudally (Franklin and Paxinos, 2008) according to standard techniques (Brown et al., 2006, 2008b). This rostrocaudal location matched the slices processed for immunohistochemistry (described above). Slices were then placed into ACSF containing (in mM): 124 NaCl, 1.8 KCl, 25.6 $NaHCO_3$, 1.2 KH_2PO_4, 2 $CaCl_2$, 1.3 $MgSO_4$ and 10 glucose (osmolarity 300 mOsm), saturated with 95% O_2/5% CO_2 for >1 hour at room temperature before being transferred to the recording chamber and superfused with warmed ACSF (32°C) at 2–3 ml/min.

In order to confirm our results in adult (1.5–3 months) mice we modified our slice preparation procedure according to the method of Zhao et al. (2011). In brief, mice were deeply anesthetized by intraperitoneal injection of pentobarbital and then transcardially perfused with 20-25 ml of ice-cold N-methyl-D-glutamine (NMDG)-solution (in mM): 92 NMDG, 2.5 KCl, 1.25 NaH_2PO_4, 30 $NaHCO_3$, 20 HEPES, 25 glucose, 2 thiourea, 5 Na-ascorbate, 3 Na-pyruvate, 0.5 $CaCl_2.4H_2O$, and 10 $MgSO_4.7H_2O$, pH 7.3, 300 mOsm. Mice were then decapitated and the brains were removed into the ice-cold NMDG-solution for 1-2 minutes. The brains were sectioned at 300-μM thickness in ice-cold NMDG-solution. Coronal slices containing BF were incubated for 15 minutes at 35°C in NMDG-solution and then transferred to a modified ACSF solution (containing in mM, 119 NaCl, 2.5 KCl, 1.25 NaH_2PO_4, 26 $NaHCO_3$, 12.5 glucose, 2 $CaCl_2.4H_2O$, 2 $MgSO_4.7H_2O$, 2 mM thiourea, 5 Na-ascorbate, and Na-pyruvate, pH 7.3, 300 mOsm.) for at least 1 hour at room temperature. The recordings were performed with our regular ACSF solution (see above).

Whole-cell recordings—Patch pipettes (3-6 MΩ) were filled with intracellular solution containing (in mM): 130 potassium gluconate, 5 NaCl, 2 $MgCl_2$, 10 HEPES, 0.1 EGTA, 2 Na_2ATP, 0.5 NaGTP, 4 MgATP, 1 spermine, 0.5% biocytin (pH 7.25 with KOH, 280 mOsm). Recordings were made using a Multiclamp 700B amplifier and pClamp 9.0 software (Axon Instruments, Foster City, CA). GABAergic (GFP+) or PV+ (Tomato+) neurons were selected for recording based on their healthy appearance under IR-DIC microscopy and their expression of the fluorescent marker. Neurons in the slices were photographed immediately prior to recording using a sensitive, black-and-white Hamamatsu ORCA-AR CCD camera. Image clarity was enhanced by adjusting the contrast and brightness in the Hamamatsu Wasabi (v. 1.5.) image processing software. Long and short-axis cell diameter was measured from these images and calibrated using a 25-μm standard grid. Membrane potential measurements were adjusted for a −15 mV liquid junction potential between pipette and bath solution (calculated using the liquid junction calculator in pClamp9.0 software). Bridge balance was adjusted after gaining access to the whole-cell and maintained throughout the experiment. Series resistance was calculated using Ohm's law based on the instantaneous response to a 5 mV hyperpolarizing current step from a holding potential of −60 mV. Recordings were accepted if series resistance was <25 MΩ (range 6–25 MΩ), action potentials were overshooting, and electrode resistance changed by less than 10% during the experiment. Sampling rate was 20 kHz.

Characterization of intrinsic membrane properties—Intrinsic membrane properties of BF GABAergic or PV+ neurons were characterized using our previously described protocols (Brown et al., 2006, 2008b). A series of 1-second long hyperpolarizing and depolarizing current pulses were applied in current-clamp from the resting membrane potential (RMP). The first hyperpolarizing step was adjusted so that the negative peak of the membrane potential during the step reached −100 mV. Progressively more depolarizing

current steps (in increments one-fifth the size of the initial step) were applied until the firing rate did not increase further. The percentage depolarizing sag was determined from the largest hyperpolarizing step as 100- [((steady state voltage at end of the step - RMP)/(peak voltage - RMP)) * 100]. To characterize hyperpolarization-activated inward currents under voltage-clamp, neurons were held at −60 mV and voltage steps from − 120 mV to −60 mV with a 10-mV increment were applied with a 10-second interval. To confirm the involvement of HCN channels in the depolarizing sag under current-clamp or the slowly developing inward current in voltage-clamp we bath-applied either the nonspecific blocker CsCl (2 mM) or the more specific agent ZD7288 (4-(N-ethyl-N-phenylamino)-1,2-dimethyl-6-(methylamino) pyrimidinium chloride, 50 μM; Ascent Scientific, Cambridge, MA). To test whether "spikelets" were due to electrical coupling we bath-applied the gap junction blocker carbenoxolone (150 μM; Sigma). Data are presented as mean ± standard error of the mean (SEM). Electrophysiological data were analyzed using pClamp 9 software (Axon Instruments, Burlingame, CA). The depolarizing sag during hyperpolarizing current pulses was fit using the Standard exponential curve fitting function (Chebyshev method) of Clampfit, with a fitting coefficient ≥0.995 being accepted as a good fit to the data. If a single exponential function did not give a good fit to the data then a second exponential function was added. Drug effects were tested using Student's *t*-test. $P < 0.05$ was considered significant.

Identification of cortically projecting BF GABAergic neurons by injections of retrograde tracer into the medial prefrontal cortex of GAD67-GFP mice—To identify cortically projecting GABA neurons, we used a retrograde tracing strategy. Heterozygous GAD67-GFP knock-in mice (age 10-12 days) were deeply anesthetized by inhalation of 3% isoflurane. Cortically projecting BF neurons were labeled by bilateral injections of the nontoxic retrograde tracer, carboxylate-modified microspheres (red/orange; 0.4 μm; F8794; Invitrogen), into the prelimbic cortex (PrL) and surrounding cortical areas (coordinates: +1.3 mm AP, 0.3 ML, −2.1 DV) using a 1-μl Hamilton microsyringe (Sigma Aldrich; Model 80100, Cat. no. 20731: needle size 25G, blunt tip) and standard stereotaxic surgical techniques. Following a survival time of 5–12 days (to allow for retrograde transport of the tracer), animals were sacrificed and coronal brain slices containing PrL (for verification of the injection site) and BF (for in vitro electrophysiological recordings) were prepared as described above. Cortically projecting BF GABAergic neurons were identified using a highly sensitive black-and-white fluorescence microscope (ORCA-AR, Hamamatsu) based on their punctate fluorescence surrounding the nucleus under the rhodamine filter set (indicating the presence of retrograde tracer) and GFP fluorescence (filling both cytoplasm and nucleus).

Post-hoc labeling for PV or ChAT—In a subset of experiments we attempted to positively identify PV+/GFP+ neurons or GFP-/ChAT+ positive neurons using immunohistochemistry. Following recording, the slice was placed in buffered 4% paraformaldehyde until processing. Slices were incubated with 1% Triton-X for 2 hours, blocked with strep-tavidin/biotin for 15 minutes each, and then treated with streptavidin-A350 (blue, Molecular Probes, Eugene, OR) at 1:100 dilution for 30 minutes to reveal the bio-cytin-containing neuron. Subsequently the slices were treated with the primary antibody for parvalbumin (rabbit; 1:200; AB11427; Abcam) or ChAT (rabbit; 1:200; AB143; Millipore) for 3 days at 4°C. To reveal the PV+ or ChAT+ neurons the slices were finally treated with donkey antirabbit IgG conjugated to AlexaFluor 594 (1:100; red; A21207; Invitrogen) for 3 hours at room temperature. Slices were examined under a fluorescence microscope.

Results

GFP selectively labeled BF GABAergic neurons of GAD67-GFP mice (Fig. 1)

In order to use GAD67-GFP knock-in mice to identify BF GABA neurons, we first confirmed that the fluorescence marker (GFP) selectively labels GABAergic neurons and no ectopic expression occurs. We performed immunohistochemical staining for GABA following bilateral colchicine injections into BF to enhance GABA levels in the cell bodies of BF GABAergic neurons (see Materials and Methods, Fig. 1A). These experiments showed that GFP was indeed a selective marker for BF GABAergic neurons in GAD67-GFP knock-in mice (Fig. 1B-D). Of the 11,165 cells analyzed in BF (four animals, three sections/animal), 87.7 ± 1.2% of GFP+ neurons were positively identified as GABAergic. Conversely, 88.4 ± 1.1% of GABAergic neurons were GFP+. Thus, the vast majority of GFP+ neurons were double-labeled with GABA, and conversely the vast majority of GABAergic neurons were GFP+. We also performed staining for the selective marker of cholin-ergic neurons, ChAT. No ChAT-positive neurons expressed GFP (Fig. 1E-G). Thus, GFP was not expressed ectopically in cholinergic neurons.

Quantification of the density, size, and colocalization of BF GFP1 (GABAergic) and PV+ neurons

In order to be able to target large, putative cortically projecting, GABAergic and PV+ neurons for in vitro elec-trophysiological studies, we quantified the relative density and size of these neurons in the BF. In particular, we focused on the following questions: 1) Where are large GABAergic neurons most densely concentrated? 2) Where are PV+ neurons most densely concentrated? 3) What percentage of PV+ neurons is GABAergic in the mouse? 4) Conversely, what percentage of BF GABAergic neurons is PV+?

Distribution of BF GABAergic neurons (Figs. 2–4)

GFP+ neurons were located throughout BF (Figs. 2, 3), but were especially concentrated in a band extending from the medial horizontal limb of the diagonal band (HDB) to the lateral magnocellular preoptic area (MCPO). In addition, many GFP+ neurons were located in the substantia innominata (SI) and ventral pallidum (VP). Although not the focus of the present study, GFP+ neurons were also present in MS/DBV, medial and lateral preoptic regions, the caudate putamen (CPu), as well as in the olfactory tubercle (Tu). In addition, green fluorescence was observed within major fiber tracts, due to the presence of GFP in axons and dendrites, causing high “background” fluorescence in the neuropil. A striking drop-off in this background fluorescence was observed at the border between pre-optic regions and BF (between the lateral preoptic nucleus [LPO] and HDB), as well as between BF and the cortex. The drop-off was particularly striking at the border of the MCPO/Tu and the piriform cortex (Fig. 2A,D,G).

The highest density of GFP+ neurons was found in the MCPO region (569.7 ± 34.6 GFP+ neurons/mm^2/slice; $n = 4$; Fig. 4), followed by the HDB (384.8 ± 28.8). More dorsal regions had a lower density (VP 191.5 ± 4.5; SI 120.4 ± 17.5). GFP+ neurons were less dense in the rostral slice when compared to the medial and caudal slices. Two-way ANOVA confirmed that there were significant differences between the four BF subnuclei ($F_{3,36} = 86.394$, $P < 0.001$), as well as between the three rostrocaudal slice representations ($F_{2,36} = 13.405$, $P < 0.001$). The interaction of these two independent variables was not significant. Follow-up pairwise comparisons revealed significant ($P < 0.001$) density differences: VP, SI < HDB, MCPO; HDB < MCPO. Significant ($P < 0.001$) density differences were found between rostral and medial (rostral < medial), and rostral and caudal slices (rostral < caudal).

Most GABAergic BF neurons were small (<15 μm long-axis diameter) or medium (15–20 μm long-axis diameter) sized (Fig. 4)

Although mean values of long-axis diameter were highest in the HDB and MCPO (VP 14.8 ± 1.0 μm, SI 15.9 ± 0.8 μm, HDB 16.3 ± 1.2 μm, MCPO 16.4 ± 1.3 μm; $n = 4$; Fig. 4B,C) and highest in caudal slices (rostral 15.5 ± 1.1 μm, medial 15.8 ± 0.9 μm, caudal 16.3 ± 1.1 μm), two-way ANOVA analysis of the long-axis diameter of GFP+ neurons did not reveal significant differences between the four BF subnuclei ($F_{3,36} = 1.946$, $P = 0.140$) or the three coronal slice representations ($F_{2,36} = 0.796$, P = 0.459). The histogram profile of BF GFP+ long-axis diameters (Fig. 4C) indicates that the vast majority of GFP+ neurons were small/medium-sized, with a small but substantial subpopulation of larger diameter (>20 μm) neurons, which likely includes the large-diameter PV+ neurons described below.

The majority of the large (>20 μm long-axis diameter) GABAergic neurons were located in ventral BF (SI, HDB, and MCPO)

Although all sizes of neurons were distributed throughout all four BF subnuclei, large-diameter neurons were more centralized in SI, HDB, and MCPO, whereas small-diameter neurons were more centralized in VP. Large GFP+ neurons made up a greater proportion of GFP+ neurons in SI (11.3 ± 5.7% of GFP+ SI neurons), HDB (12.5 ± 5.9%), and MCPO (12.9 ± 7.4%), when compared to VP (8.8 ± 4.2%). Conversely, small GFP+ neurons made up a greater proportion of GFP+ neurons in VP (52.9 ± 10.5%), compared to SI (41.7 ± 10.1%), HDB (35.0 ± 10.3%), and MCPO (36.7 ± 8.7%). Large neurons made up a greater percentage of neurons in medial (11.9 ± 6.2%) and caudal slices (13.4 ± 5.6%) when compared to rostral slices (8.8 ± 5.5%). Therefore, in order to target putative cortically projecting BF GABAergic neurons we centralized our electrophysiological recordings of large-sized GFP+ neurons in SI, HDB, and MCPO in medial and caudal BF slices (see below).

PV labeled a subpopulation of GABAergic neurons in the BF (Figs. 2, 3, 5)

Previous studies in the rat demonstrated the presence of PV in a subset of large GABAergic neurons projecting to the cortex (Gritti et al., 2003). To determine if PV labels a sub-population of GABAergic neurons in the mouse, we performed immunohistochemistry for PV in GAD67-GFP knock-in mice. Indeed, in tissue sections labeled for PV, a subpopulation of GFP+ neurons in the BF was PV+, intermingled among many PV stained fibers (Fig. 2). Three primary clusters of PV+ neurons were evident in VP, ventromedial (HDB), and ventrolateral (MCPO) BF regions (Figs. 2, 3, 5A).

The highest density of PV+ neurons was in MCPO (Fig. 5A); PV+ BF neurons were predominantly of medium (15–20 μm long-axis diameter) and large (>20 μm long-axis diameter) size (Fig. 5B,C)

Quantification of the density (Fig. 5A) of BF PV+ neurons confirmed that the highest density of PV+ neurons was found in the MCPO (54.1 ± 6.8 PV+ neurons/mm^2/slice; $n = 4$), followed by VP (26.3 ± 3.6) and HDB (16.0 ± 4.9), with the lowest density in SI (13.4 ± 2.9). Lower densities of BF PV+ neurons were found in the rostral BF (20.3 ± 6.4 PV+ neurons/mm^2/slice; $n = 4$) when compared to medial (40.1 ± 10.9) and caudal BF (32.8 ± 10.6). Two-way ANOVA revealed that there were significant differences between the four BF subnuclei ($F_{3,36} = 11.845$, $P < 0.001$), as well as between the three rostro-caudal slice representations ($F_{2,36} = 8.501$, $P = 0.001$). The interaction of these two independent variables was not significant. Follow-up pairwise comparisons revealed significant density differences: VP < MCPO ($P = 0.023$); SI, HDB < MCPO ($P < 0.001$). Significant density differences between rostral and medial slices (rostral < medial, $P = 0.003$), and medial and

caudal slices (medial > caudal, $P = 0.003$). Therefore, lowest densities of PV+ neurons were observed in rostral BF, and highest densities were in medial/caudal MCPO.

The mean values of PV+ neuronal long-axis diameters were quantified for each subnucleus (Fig. 5B; VP 18.8 ± 0.5 μm, SI 20.5 ± 0.7 μm, HDB 20.6 ± 0.9 μm, MCPO 20.8 ± 0.9 μm; $n = 4$) and the three rostrocaudal coronal representations (rostral 19.7 ± 0.6 μm, medial 20.4 ± 1.0 μm, caudal 20.4 ± 0.9 μm). Two-way ANOVA analysis of the long-axis diameter of PV+ neurons revealed significant differences between the four BF subnuclei ($F_{3,36} = 4.295$, $P = 0.011$), but not between the three rostrocau-dal slice representations ($F_{2,36} = 1.100$, $P = 0.344$). The interaction of these two independent variables was not significant. Follow-up pairwise comparisons revealed significant differences: VP < HDB ($P = 0.046$), VP < MCPO ($P = 0.02$), and VP and SI differences approached significance (VP < SI, $P = 0.053$). Thus, the mean PV+ long-axis diameter was significantly smaller in VP, compared to the other BF subnuclei.

A histogram of BF PV+ long-axis diameters (Fig. 5C) revealed that most PV+ neurons were of large (>20 μm long-axis diameter, 51.7 ± 5.7%) or medium size (15–20 μm, 41.7 ± 5.8%), with a low percentage of small neurons (<15 μm, 6.7 ± 0.8%). Large PV+ neurons made up a greater proportion of PV+ neurons in SI (54.2 ± 9.3%), HDB (59.2 ± 9.8%), and MCPO (58.3 ± 9.8%), when compared to VP (35 ± 9.6%). Conversely, small PV+ neurons made up a slight proportion of PV+ neurons in VP (6.7 ± 1.8%), SI (6.3 ± 4.6%), HDB (8.8 ± 2.1%), and MCPO (5.0 ± 2.3%). Large neurons made up a large percentage of neurons in rostral (45.9 ± 9.2%), medial (55.3 ± 10.0%), and caudal slices (53.8 ± 8.4%).

Colocalization of PV and GABA (Fig. 5D)

Immunohistochemistry for PV revealed that a high percentage (66.8%) of PV+ neurons in the BF were also GFP+ (Fig. 5D). 62.0 ± 2.2% of PV+ neurons were also GFP+ in VP; 66.0 ± 2.3% in SI; 66.9 ± 6.0% in HDB; and 72.2 ± 1.1% in MCPO. Two-way ANOVA analysis of the percentages of PV+ neurons which were GFP+ did not reveal any significant differences between the four subnuclei ($F_{3,36} = 0.396$, $P = 0.757$) or between the three coronal slice representations ($F_{2,36} = 1.235$, $P = 0.303$).

When considering the percentage of all BF GABAergic neurons that were PV+, only 6.7% of BF GFP+ neurons were also PV+ (9.6 ± 0.7% in VP; 6.8 ± 0.4% in SI; 3.4 ± 0.9% in HDB; and 6.8 ± 0.4% in MCPO). However, when considering the subpopulation of large GFP+ neurons (>20 μm, which we targeted for electrophysiological recordings), a much higher percentage (24.2%) were also PV+ (25.7% in MCPO, 9.5% in HDB, 27.9% in SI, 22.5% in VP).

Intrinsic membrane properties of BF neurons (Figs. 6 – 8)

In order to identify the properties of putative, cortically projecting, BF GABAergic neurons for the first time, we performed whole-cell recordings from large (>20 μm diameter) GFP+ neurons of HDB, MCPO, and SI in coronal brain slices prepared from GAD67-GFP knock-in mice. For comparison, we also recorded a lower number of small (<20 μm long-axis diameter) GFP+ neurons and a subpopulation of large, GFP-negative neurons ($n = 26$) which had the intrinsic membrane properties of cholinergic neurons. For this GFP-negative subpopulation, following recording, we performed staining for ChAT. In all slices ($n = 13$) where we were able to identify the biocytin-filled neuron, the neuron was double-labeled for ChAT, confirming that they were indeed cholinergic (Fig. 6A-C).

BF cholinergic neurons were slow firing, with broad action potentials, whereas large GABAergic neurons were spontaneously active with high maximal firing frequencies and brief action potentials (Fig. 6)

Large BF GFP+ neurons (n = 166) were usually triangular or fusiform in shape and had intrinsic membrane properties that were distinctly different from cholinergic neurons (Fig. 6D-F). The vast majority of large GFP+ neurons (n = 153/166) were spontaneously active and fired at a high rate (12.9 ± 0.8 Hz, n = 153), whereas cholinergic neurons were either silent at rest (n = 15) or fired slowly (1.1 ± 0.5, n = 11). Consistent with the higher spontaneous firing frequency of large GFP+ neurons, they had a significantly more depolarized resting membrane potential (RMP, −63.3 ± 0.6 mV) than cholinergic neurons (−71.5 ± 1.0 mV; P < 0.0001). The maximal firing frequency of large GFP+ neurons (87 ± 5 Hz) was also significantly higher (P < 0.0001) than cholinergic neurons (14 ± 1 Hz), likely due to the significantly larger afterhyperpolarizations (AHPs) in cholinergic neurons (large GFP+ neurons −15.3 ± 0.3 mV; cholinergic neurons −26.4 ± 1.0 mV, P < 0.0001). Cholinergic neurons exhibited other distinctive features identified in previous studies such as a shoulder on the falling phase of the action potential (not shown), resulting in a broader action potential (action potential width at half-maximal amplitude: 0.80 ± 0.06 ms vs. 0.61 ± 0.02 ms in large GFP+ neurons, P < 0.001) and a modest potassium-dependent rectification during hyperpolarizing current pulses (Fig. 6A-C). Overall, GFP-negative cholinergic neurons could be characterized as slow-firing neurons with broad action potentials, whereas large GFP+ neurons were fast-firing, spontaneously active neurons with brief action potentials (Table 2).

Large GABAergic BF neurons exhibited a prominent depolarizing sag during hyperpolarizing current pulses mediated by I_h; two subgroups (large I_h, small I_h) differed in the size and kinetics of the sag (Figs. 6, 7)

All large GFP+ neurons exhibited a striking depolarizing sag during hyperpolarizing current injection (Fig. 6D-F). However, the kinetics and amplitude of this sag differed considerably between individual neurons (Fig. 7A–H, Table 2). We subdivided the neurons into two subgroups based on whether the depolarizing sag following a step to −110 mV (largest step tested) was best fit by a monoexponential or biexponential curve. Neurons whose sag was fit by a biexponential curve (n = 89, τ_{fast} = 53.1 ± 0.8 ms; τ_{slow} = 574 ± 90 ms) had a larger sag (52.9 ± 1.1%), whereas those fit with a monoexponential curve (n = *77*, τ = 472 ± 191 ms) had a smaller but still substantial sag (28.1 ± 1.0%; P < 0.0001). Pharmacological experiments (described next) suggested that the sag in both groups was mediated by activation of hyperpolarization-activated currents (I_h). Thus, we termed these two groups of neurons large I_h (biexponential decay) and small I_h (monoexponential decay). In all, 80 of 89 large I_h neurons fired spontaneously (in the absence of injected current) at a frequency of 15.0 ± 1.2 Hz, while 64 of *77* small I_h neurons fired spontaneously. Those that did fire had a frequency of 10.2 ± 1.0 Hz. In neurons exposed to tetrodotoxin (TTX; 0.5 μM), large I_h neurons had a more depolarized RMP of −61.5 ± 0.7 mV (n = 47) whereas small I_h neurons had an RMP of −65.4 ± 0.8 mV (n = 39). Large I_h neurons had a higher spontaneous firing frequency (P < 0.01), a more depolarized RMP (P < 0.001), and a lower input resistance (P < 0.0001) than small I_h neurons. Large I_h neurons had slightly broader action potentials (P = 0.034) and smaller AHPs (P = 0.0005) than small I_h neurons (Table 2).

We investigated the mechanism underlying the depolarizing sag observed in large GFP+ neurons using pharmacological tools in both current and voltage-clamp (Fig. 7A–H). In current-clamp, the sag was blocked in both large I_h and small I_h neurons by application of the nonspecific blocker of hyperpolarization-activated, cyclic-AMP regulated, cation (HCN) channels, cesium chloride (2 mM; n = 8; 4 large I_h, 4 small I_h) and by the more specific I_h blocker ZD7288 (100 μM, n = 7; 4 large I_h, 3 small I_h). ZD7288 also hyperpolarized large I_h

neurons from −69.1 ± 0.8 mV to −71.5 ± 1.4 mV (−2.4 ± 0.7 mV, $n = 4$; $P < 0.05$), whereas the membrane potential of small I_h neurons was not significantly affected (from −73.6 ± 0.4 mV to −73.3 ± 0.4 mV, $n = 3$). Under voltage-clamp, 1-second steps to −120 mV from a holding potential of −60 mV induced a slowly developing inward current in both types of neurons. Large I_h neurons had a maximal inward current at the end of the step of −479.2 ± 56.2 pA ($n = 8$). After the neurons were incubated in ZD7288 (50 μM) for 10 minutes, the holding current at −60 mV changed from −303.3 ± 44.7 pA to −153.7 ± 26.9 pA ($P = 0.0095$, paired t-test, $n = 8$), resulting in an outward current of 149.6 ± 42.3 pA, indicating that I_h channels are open close to the resting membrane potential. ZD7288 significantly decreased the amplitude of the I_h current to −97.1 ± 15.7 pA ($P = 0.0004$, paired t-test). Small I_h neurons had a significantly smaller inward current (−58.0 ± 23.5 pA at − 120 mV, $n = 8$) compared to large I_h neurons ($P < 0.0001$, unpaired t-test). ZD7288 did not significantly change the baseline current at −60 mV (ACSF vs. ACSF + ZD7288: −111.5 ± 36.5 pA vs. −101.8 ± 26.1 pA, $P = 0.4306$, paired t-test, $n = 8$) but significantly decreased the I_h current to −11.5 ± 7.0 pA ($P = 0.0447$). Thus, all large GFP+ neurons have a depolarizing sag which is mediated by a hyperpolarization-activated cation current. In large I_h neurons, this current is active at the resting membrane potential.

During depolarizing current pulses, large GFP+ neurons fired tonically with little adaptation. The adaptation ratio, calculated as the number of action potentials during the last 100 ms of the first depolarizing current pulse divided by the number of action potentials during the first 100 ms of the same step was 0.70 ± 0.02 in large I_h neurons and 0.77 ± 0.04 in small I_h neurons.

The expression of voltage-gated channels can change during development. Therefore, we characterized the properties of a smaller group of large GFP+ neurons ($n = 5$ large I_h neurons, $n = 5$ small I_h neurons) in older animals (1.5–3 months, see Materials and Methods). The intrinsic membrane properties were very similar in recordings from these older animals. In particular, the neurons had depolarized RMPs (large I_h −65.4 ± 1.3 mV; small I_h − 68.6 ± 2.2 mV), fast spontaneous firing (large I_h 20.4 ± 4.6 Hz; small I_h 7.7 ± 5.7 Hz), a high maximal firing rate (large I_h 126 ± 17 Hz; small I_h 87 ± 22 Hz), brief action potentials (action potential half-width: large I_h 0.58 ± 0.03 ms; small I_h 0.62 ± 0.06 ms) and a prominent depolarizing sag (Sag%: large I_h 57.1 ± 3.4; small I_h 32.9 ± 9.3). These values were not significantly different from those in young animals. Thus, the intrinsic membrane properties of large BF GABA neurons do not appear to change in the developmental period from 12 days to 3 months.

Large GABAergic neurons may be electrically coupled (Fig. 8)

One interesting feature of large BF GABAergic neurons was the presence of subthreshold fluctuations in the membrane potential when the neurons were hyper-polarized below the threshold for action potential generation or when they were firing slowly (Fig. 8). In neurons where these events were well resolved these events had a quite different time course (Fig. 8B) to spontaneously occurring excitatory postsynaptic potentials (Fig. 8C). They resembled small, low-pass filtered action potentials and were thus termed “spikelets.” These events were observed most commonly in large I_h neurons (25%, 22/89 neurons) and only rarely in small I_h neurons (3%; 2/77 neurons). They were abolished by TTX, indicating that they require the activity of voltage-gated sodium channels. These events could represent “ectopic” action potentials generated away from the somatic recording electrode or could be due to action potentials in neighboring, electrically coupled cells, filtered by the low-pass characteristics of gap junctions. To directly test for an involvement of gap junctions we investigated the effect of the gap junction blocker carbenoxolone (150 μM). Carbenoxolone blocked the spikelets ($n = 6/6$) and also increased the input resistance from 62.0 ± 6.2 MΩ to 121.0 ± 20.1 MΩ ($P = 0.029$, paired t-test, $n = 6$, Fig. 8D), suggesting that the spike-lets

were due to electrical coupling and not to ectopic action potentials. Interestingly, neurons with spikelets had a higher spontaneous firing frequency than those without spikelets. Large I_h neurons with spikelets had a firing frequency of 21.7 ± 1.8 Hz, whereas neurons without spikelets had a frequency of 12.4 ± 1.3 Hz ($P < 0.01$) were not significantly different ($P > 0.05$) than their spikelet frequency suggesting that the spikelets were driving the high spontaneous firing frequency of these neurons.

One subpopulation of small/medium sized GABAergic neurons exhibit intrinsic membrane properties similar to striatal medium spiny neurons (Fig. 7)

Although not the main focus of this study, our anatomical studies suggested that most BF GABAergic neurons are small or medium-sized neurons. Therefore, we also characterized the intrinsic membrane properties of small-to-medium sized (<20 μm) BF GFP+ (GABAergic) neurons. These neurons either had intrinsic membrane properties similar to small I_h neurons ($n = 12$) or exhibited intrinsic membrane properties similar to striatal medium spiny neurons (Blomeley and Bracci, 2008). This group of GFP+ neurons ($n = 19$, Fig. 7I-L, Table 2) consisted of small (long-axis diameter 14.2 ± 0.5 μm), round/ovoid shaped cells, which were silent at rest with a resting membrane potential (−77.7 ± 1.5 mV) which was significantly more hyperpolarized than in the large GFP+ neurons ($P < 0.0001$). In contrast to the large GFP+ neurons, but similar to medium spiny neurons, this group of neurons exhibited a time-independent inward rectification during hyperpolarizing current pulses which was abolished by the blocker of inwardly rectifying potassium channels $BaCl_2$ (100 μM, $n = 7$ current-clamp, $n = 5$ voltage-clamp, Fig. 7K,L). This type of neuron was also found in Tu and VP (data not shown) regions that gene expression studies (e.g., dopamine D2 receptor, Allen Mouse Brain Atlas; http://mouse.brain-map.org) suggest are anatomically similar to the striatum. In comparison to the GFP-negative, cholinergic neurons the GFP+ medium-spiny like neurons were smaller ($P < 0.0001$), had a more negative RMP ($P = 0.0013$), a smaller input resistance ($P = 0.0080$), and higher maximal firing rates ($P = 0.0056$).

Cortically projecting BF GABAergic neurons exhibited intrinsic membrane properties identical to large GABAergic BF neurons (Fig. 9)

As described above, we focused our recordings on large GFP+ neurons since previous work in the rat suggested that cortically projecting BF GABAergic neurons are predominantly large neurons (Gritti et al., 1997). To more directly ascertain the intrinsic membrane properties of cortically projecting GABAergic neurons, we stereotaxically injected nontoxic rhodamine latex microspheres (RLM) into the frontal cortex (prelimbic cortex and surrounding areas) in young mouse pups (10–14 days) in order to retrogradely label neurons in the BF (Fig. 9A,B). Following a survival period of 5–12 days we prepared BF slices and selected neurons for recording based on their expression of GFP and punctate rhodamine fluorescence. In 4 of 12 mice pups injected with RLM we obtained large injections covering a large proportion of the prefrontal cortex and could observe RLM in individual BF neurons. In these mice we recorded nine retrogradely labeled, GFP+ neurons. Cortically projecting, GFP+ neurons were fast firing, with a prominent depolarizing sag during hyperpolarizing current pulses (Fig. 9C). Four of the neurons were characterized as large I_h neurons (biexponential decay, Fig. 9C) and five were characterized as small I_h (monoexponential decay, not shown). These intrinsic membrane properties were essentially identical to the large GFP+ neurons (Table 2). No significant differences were found in the intrinsic membrane properties when comparing large I_h GFP+ neurons and large I_h GFP+ neurons which were cortically projecting or small I_h GFP+ neurons and small I_h GFP+ neurons which were cortically projecting, except that the AHP was slightly larger in cortically projecting large I_h neurons (−21.4 ± 3.4 mV vs. − 16.6 ± 0.5 MΩ; $P = 0.0016$).

PV+ BF neurons identified by post-hoc immunohistochemistry in GAD67-GFP knock-in mice or expression of the red fluorescent marker Tomato in PV-Tomato mice have similar properties to large and cortically projecting GABAergic neurons (Figs. 9, 10) but exhibit narrower action potentials and a higher maximal firing frequency

A large proportion of cortically projecting BF GABAergic neurons contain PV in the rat (Gritti et al., 2003; Furuta et al., 2004). Therefore, we attempted to immunohistochemically label recorded neurons post-hoc for PV and biocytin. Although PV staining was successful in slices fixed following recording, using this method we only rarely successfully encountered PV+ neurons (n = 2/40, Fig. 9D-F) that were also biocytin-positive, even though GFP+/PV+ neurons with a similar size and morphology were often located close to the recorded cell. The intrinsic membrane properties of the two GFP+/PV+ neurons we recorded were similar to cortically projecting BF GABA neurons (Fig. 9).

To obtain a larger number of recordings from identified PV+ neurons we used a different strain of mice (PV-Tomato, see Materials and Methods) where the expression of a red fluorescent marker (Tomato) is driven by the PV promoter. Immunohistochemical staining for PV in sections from PV-Tomato mice confirmed that Tomato specifically labels PV+ neurons in the BF (Fig. 10A-F). 86.2 ± 1.8% of Tomato Positive neurons were labeled with PV antibody (n = 3 animals, 3 slices per case). Overall, PV labeling in BF was very similar to that observed following PV immunohistochemistry in the GAD67-GFP knock-in mice described above. In the ventral BF the main cluster of PV+ neurons was found in the lateral MCPO. Thus, we focused on this area for our electrophysiological recordings.

Whole-cell recordings from Tomato+ neurons in these mice revealed two populations of neurons with intrinsic membrane properties very similar to the large I_h and small I_h groups recorded in the GAD67-GFP knock-in mice (Fig. 10G-L). Large I_h PV+ neurons (Fig. 10G-I, n = 6, Table 2) had a cell size of 24 ± 1.1 μm, a resting membrane potential of −63 ± 1.3 mV, a depolarizing sag of 51.8 ± 2.4% with a biexponential decay (τ_{fast} = 42.0 ± 4.7 ms; τ_{slow} = 464 ± 83 ms), a spontaneous firing frequency of 15.6 ± 6.6 Hz, and a maximum firing frequency of 162 ± 18 Hz. One large I_h PV-positive neuron exhibited spike-lets. Small I_h PV neurons (Fig. 10J-L, n = 6) had a cell size of 24.8 ± 1.1 μm, a resting membrane potential of −66 ± 0.9 mV, a depolarizing sag: 67.6 ± 2.2% with a monoexponential decay (τ = 200.5 ± 26.9 ms), a spontaneous firing frequency of 21 ± 5.5 Hz, and a maximum firing frequency of 164 ± 76 Hz.

Mean data for the intrinsic membrane properties of the neurons recorded in this study are provided in Table 2. A summary of the intrinsic membrane properties of individual PV+ neurons and a comparison with those of GFP+ and GFP+ cortically projecting neurons is provided in Figure 11. When comparing the resting membrane potentials, spontaneous firing frequencies, input resistances, and depolarizing sag characteristics of large I_h GFP+ and large I_h PV+ neurons, no significant differences were found. Similarly, these parameters did not differ when comparing GFP+ small I_h neurons and PV+ small I_h neurons. However, PV + neurons from PV-Tomato mice had briefer action potentials (AP half-width: 0.27 ± 0.02 ms vs. 0.61 ± 0.02 ms of large GFP^+ neurons, $P < 0.0001$) and had higher maximal firing frequencies than large GFP+ neurons recorded in GAD67-GFP knock-in mice (163 ± 37 Hz vs. 87 ± 5 Hz of large GFP+ neurons, $P = 0.0002$).

Discussion

The main advances reported in this study are as follows: 1) Validation of novel genetic tools to investigate the anatomy and physiology of BF GABAergic and PV+ neurons involved in behavioral state control; 2) The first comprehensive mapping of the distribution of GABAergic and PV+ BF neurons in the mouse; and 3) The first description of the intrinsic

membrane properties of identified BF GABAergic neurons, including the subpopulations which are PV+ and cortically projecting.

GAD67-GFP mice can be used to reliably identify BF GABAergic neurons

Staining of GABAergic neurons in many subcortical regions is challenging due to low levels of GAD67/GABA in the cell bodies and poor penetration of antibodies. To circumvent these problems of identification, different strategies have been used to create transgenic mice expressing fluorescent proteins in GABAergic neurons (Oliva et al., 2000; Tamamaki et al., 2003; Chattopadhyaya et al., 2004). Use of random insertion (Oliva et al., 2000) or bacterial artificial chromosome (BAC) (Chattopadhyaya et al., 2004) may not selectively label all GABAergic neurons since the inserted transgene is inserted in an ectopic position in the genome and may be under the control of nonnative upstream elements, resulting in either incomplete or ectopic expression. Knock-in mice, such as the GAD67-GFP knock-in mice used here, do not have these problems since the coding sequence for GFP is inserted in the native position in the genome (Tamamaki et al., 2003). In fact, in our experiments GFP was detectable in the vast majority of BF GABAergic neurons, and ectopic expression was not observed in cholinergic neurons. The small percentage of GFP+ cells not labeled by GABA was likely due to poor antibody penetration or low levels of GABA antigen in the cell bodies (despite colchicine pretreatment). Conversely, the finding that ~12% of GABAergic neurons did not express detectable levels of GFP is similar to other brain areas studied in these mice (Tamamaki et al., 2003; Brown et al., 2008b) and corresponds to findings from other GFP-expressing strains (e.g., orexin GFP mice; Li et al., 2002). One potential disadvantage of knock-in animals is that the targeted gene is knocked-out, resulting in changes in the behavior being studied. However, the heterozygous GAD67-GFP knock-in animals used here have sleep patterns and EEG rhythms that are not noticeably different from those in wildtype animals (Chen et al., 2010). When considered together with previous studies (Tamamaki et al., 2003; Brown et al., 2008b; McKenna et al., 2010; McNally et al., 2011), our results suggest that GAD67-GFP knock-in mice can be used to study GABAergic neurons involved in sleep-wake control throughout the brain.

Neuroanatomical characterization of BF GABAergic neurons in the mouse

Detailed mapping of the location of BF GABAergic neurons revealed that GABAergic neurons were located in all four subregions of the BF studied here, as well as in neighboring preoptic regions. Although not described in this study, GABAergic neurons were also evident in the MS/DBV and magnocellular basal nucleus. Of the four subnuclei investigated, GABAergic neurons were most densely concentrated in the MCPO and HDB regions, as in the rat (Brashear et al., 1986; Gritti et al., 1993). Previous reports demonstrated that BF GABAergic neurons have long diameter axes of ~10–30 μm in the cat (Fisher et al., 1988) and rat (Gritti et al., 1993, 1997). The majority of GABAergic neurons in the rat BF were small/medium-sized neurons (~15 μm in large diameter), similar to our results here in the mouse (overall long axes diameter average of 15.9 μm across all four BF subnuclei studied here). These smaller diameter GABAergic neurons may act as local interneurons, or projection neurons that descend to the lateral hypothalamus (Gritti et al., 1994). Larger diameter GABAergic neurons in the rat and cat BF were largely located in HDB and MCPO (Zaborszky et al., 1986a,b; Fisher et al., 1988; Gritti et al., 1993), as reported here in the four subnuclei investigated (mean long axes diameter of 16.4 μm for both HDB and MCPO). This smaller but still substantial subgroup of larger GABAergic diameter neurons, similar to the size of BF cholinergic neurons, likely project to the cerebral cortex (Fisher et al., 1988; Smith et al., 1994; Gritti et al., 1997).

Large, cortically projecting BF GABAergic neurons are fast firing neurons with prominent H-currents, electrical coupling, and are most dense in the MCPO

Large BF GABAergic neurons were spontaneously active, fast-firing neurons with brief action potentials. Recordings from identified cortically projecting GABAergic neurons revealed essentially identical intrinsic membrane properties, similar to previous recordings from cortically projecting, unidentified noncholinergic BF neurons (Furuta et al., 2004; Arrigoni et al., 2010). In contrast, cholinergic neurons were mainly silent, fired at low frequencies when depolarized, and had broad action potentials.

One distinguishing property of large, GABAergic neurons was a time-dependent inward rectification when hyperpolarized, which was abolished by the H-current blockers cesium and ZD7288, indicating that it was due to an inward current through HCN channels. Prominent H-currents are often found in neurons exhibiting rhythmic activity since the H-current provides a depolarizing drive in the intraburst interval. Thus, the rhythmic clusters or burst firing observed in vivo recordings from GABAergic neurons whose firing is correlated with cortical activation (Manns et al., 2000; Duque et al., 2000; Hassani et al., 2009) may reflect the activation of the H-current. Detailed analysis revealed two subgroups according to the amount and kinetics of the depolarizing sag. Large I_h neurons had a more depolarized RMP and lower input resistance. In these neurons, ZD7288 caused a hyperpolarization in current-clamp and induced an outward current in voltage-clamp, indicating that the H-current in these neurons contributes to this depolarized resting membrane potential and high spontaneous firing frequency. These two subgroups also differed in their expression of spikelets and in their pharmacology (Franciosi et al., 2008; Yang et al., 2011). Differences in kinetics may reflect different HCN subunits combinations. In situ hybridization in mouse brain coronal sections (Allen Brain Atlas; http://mouse.brain-map.org) indicates the presence of HCN1 and 2 channels in the HDB and MCPO regions where GABAergic neurons are concentrated. Similarly, immunohistochemical staining revealed the presence of HCN1 channels on a subpopulation of rhythmically firing, medial septal GABAergic/PV+ neurons (Varga et al., 2008). HCN1 channels have faster kinetics and thus may account for the depolarizing sag in the large I_h neurons. Interestingly, HCN1/2 channels are targets for inhalational anesthetics at clinically relevant concentrations (Chen et al., 2005). Thus, inhibition of cortically projecting BF GABAergic neurons may be one target for these agents.

One novel finding of this study was that large BF GABAergic neurons, especially large I_h neurons, exhibited subthreshold oscillations (spikelets). Neurons exhibiting prominent spikelets had a lower input resistance, suggesting additional channels are open at the resting membrane potential. The gap junction blocker carbenoxolone blocked the spikelets and increased the input resistance. Thus, these events likely reflect current flow due to action potentials in neighboring, spontaneously active BF GABAergic neurons that are connected through electrical synapses. Interestingly, electrical coupling is also a typical feature of GABAergic interneurons in the cerebral cortex (Galarreta and Hestrin, 2002). Such coupling provides a mechanism to synchronize the firing of this group of neurons and thereby amplify their effect on their cortical targets.

Subpopulation of small/medium sized neurons has similar properties to striatal projection neurons

As described above, most GABAergic neurons were small-to-medium sized neurons, likely interneurons or caudally projecting. The small-to-medium sized neurons that lacked I_h were characterized by a strong time-independent inward rectification which was abolished by the I_{Kir} blocker barium (Gerber et al., 1989) as in group II BF noncholinergic neurons recorded by Arrigoni et al. in the rat (2006). Their properties were reminiscent of GABAergic

medium-spiny projection neurons in the striatum (Blomeley and Bracci, 2008). This group of neurons had a hyperpolarized resting membrane potential and was unresponsive to wake promoting neurotransmitters (unpubl. obs.) suggesting that they are likely to have either sleep-active or state-indifferent firing patterns.

Identified BF PV+ neurons are mainly GABAergic and have similar membrane properties to large and cortically projecting BF GABA neurons

In our study, the majority (~67%) of BF PV+ neurons were GFP+. This number is likely to underestimate the percentage of PV+ neurons that are GABAergic since GFP was undetectable in ~12% of GABAergic neurons. Overall, this number (79%) approximates the percentage of GABA/PV+ neurons in the rat (~90%; Gritti et al., 2003). The mean long axis diameter of PV+ neurons in BF was 20.2 μm, which is substantially larger than the mean diameter of GABAergic neurons (15.9 μm). Thus, as in the rat, PV is a marker for a subpopulation of large GABAergic neurons. The intrinsic membrane properties of PV+ neurons were overall very similar to those of large or cortically projecting GABAergic neurons. They were also similar to those of identified PV+ neurons in the rostral part of the BF containing neurons projecting to the hippocampus (Morris et al., 1999), suggesting commonality of function. Similar to the cortical PV+ interneurons to which they project, BF PV+ neurons have very narrow action potentials and the highest maximal firing frequencies. Thus, PV+ neurons may correspond to the subpopulation of BF GABAergic neurons that are most active during states associated with cortical activation, i.e., waking and paradoxical (REM) sleep (WP-max neurons) and exhibit firing in bursts with frequencies exceeding 80 Hz (Hassani et al., 2009). In contrast to cortical PV+ neurons, BF PV+ neurons have a prominent depolarizing sag during hyperpolarizing current pulses which may be important for generating rhythmic firing.

Functional implications

The intrinsic membrane properties and forebrain projection targets of BF GABA/PV+ neurons predispose them towards a role in control of fast EEG rhythms in the gamma range. Previous reports showed that BF GABAergic or PV+ cells project to and synapse onto GABA/PV+ neurons in forebrain structures that generate gamma oscillations, namely, the neocortex (Freund and Meskenaite, 1992; Gritti et al., 2003; Henny and Jones, 2008), thalamic reticular nucleus (Bickford et al., 1994), and amygdala (McDonald et al., 2011). Accordingly, ibotenate lesions of the BF decreased cortical fast rhythms and these effects were correlated with the loss of PV+ neurons (Kaur et al., 2008; Fuller et al., 2011). Study of this inhibitory, GABAergic, component of the ascending reticular activating system may enable the development of novel drugs which promote or inhibit cortical activation.

Supplementary Material

Refer to Web version on PubMed Central for supplementary material.

Acknowledgments

We thank Dr. Robert E. Strecker for the support of his VA MERIT grant.

Grant sponsor: Department of Veterans Affairs Medical Research Service Award (to R.W. McCarley); NIMH; Grant number: R01 MH039683; Grant sponsor: NHLBI; Grant number: HL095491 (to R.W. McCarley); Grant sponsor: NIMH; Grant number: R21 MH094803 (to R.E. Brown); Grant sponsor: Grants-in-Aids for Scientific Research from MEXT, Japan and Takeda Science Foundation (to Y. Yanagawa).

Literature Cited

Akgul G, Wollmuth LP. Expression pattern of membrane-associated guanylate kinases in interneurons of the visual cortex. J Comp Neurol. 2010; 518:4842–4854. [PubMed: 21031555]

Arrigoni E, Chamberlin NL, Saper CB, McCarley RW. Adenosine inhibits basal forebrain cholinergic and noncholinergic neurons in vitro. Neuroscience. 2006; 140:403–413. [PubMed: 16542780]

Arrigoni E, Mochizuki T, Scammell TE. Activation of the basal forebrain by the orexin/hypocretin neurones. Acta Physiol (Oxf). 2010; 198:223–235. [PubMed: 19723027]

Bickford ME, Gunluk AE, Van Horn SC, Sherman SM. GABAergic projection from the basal forebrain to the visual sector of the thalamic reticular nucleus in the cat. J Comp Neurol. 1994; 348:481–510. [PubMed: 7836559]

Blomeley C, Bracci E. Substance P depolarizes striatal projection neurons and facilitates their glutamatergic inputs. J Physiol. 2008; 586:2143–2155. [PubMed: 18308827]

Bowser DN, Khakh BS. ATP excites interneurons and astrocytes to increase synaptic inhibition in neuronal networks. J Neurosci. 2004; 24:8606–8620. [PubMed: 15456834]

Brashear HR, Zaborszky L, Heimer L. Distribution of GABAergic and cholinergic neurons in the rat diagonal band. Neuroscience. 1986; 17:439–451. [PubMed: 3517690]

Brischoux F, Mainville L, Jones BE. Muscarinic-2 and orexin-2 receptors on GABAergic and other neurons in the rat mesopontine tegmentum and their potential role in sleep-wake state control. J Comp Neurol. 2008; 510:607–630. [PubMed: 18709662]

Brown RE, Thakkar MM, Winston S, Basheer R, Yanagawa Y, McCarley RW. Electrophysiological characterization of neurons in the dorsolateral pontine rapid-eye-movement sleep induction zone of the rat: intrinsic membrane properties and responses to carbachol and orexins. Neuroscience. 2006; 143:739–755. [PubMed: 17008019]

Brown RE, Franciosi S, McKenna JT, Winston S, Yanagawa Y, McCarley RW. Electrophysiological recordings from GABAergic neurons in GAD67-GFP knock-in mice expressing green fluorescent protein under the control of the glutamic acid decarboxylase 67 promoter. Sleep. 2007; 30:A22.

Brown RE, Franciosi S, McKenna JT, Winston S, Yanagawa Y, McCarley RW. Electrophysiological and pharmacological characterization of cortically projecting basal forebrain neurons in the mouse. Soc Neurosci Abs. 2008a; 384:16.

Brown RE, McKenna JT, Winston S, Basheer R, Yanagawa Y, Thakkar MM, McCarley RW. Characterization of GABAergic neurons in rapid-eye-movement sleep controlling regions of the brainstem reticular formation in GAD67-green fluorescent protein knock-in mice. Eur J Neurosci. 2008b; 27:352–363. [PubMed: 18215233]

Burk JA, Sarter M. Dissociation between the attentional functions mediated via basal forebrain cholinergic and GABAergic neurons. Neuroscience. 2001; 105:899–909. [PubMed: 11530228]

Buzsaki G, Bickford RG, Ponomareff G, Thal LJ, Mandel R, Gage FH. Nucleus basalis and thalamic control of neocortical activity in the freely moving rat. J Neurosci. 1988; 8:4007–4026. [PubMed: 3183710]

Cape EG, Jones BE. Effects of glutamate agonist versus procaine microinjections into the basal forebrain cholinergic cell area upon gamma and theta EEG activity and sleep-wake state. Eur J Neurosci. 2000; 12:2166–2184. [PubMed: 10886356]

Cardin JA, Carlen M, Meletis K, Knoblich U, Zhang F, Deisseroth K, Tsai LH, Moore CI. Driving fast-spiking cells induces gamma rhythm and controls sensory responses. Nature. 2009; 459:663–667. [PubMed: 19396156]

Chang SY, Zagha E, Kwon ES, Ozaita A, Bobik M, Martone ME, Ellisman MH, Heintz N, Rudy B. Distribution of Kv3.3 potassium channel subunits in distinct neuronal populations of mouse brain. J Comp Neurol. 2007; 502:953–972. [PubMed: 17444489]

Chattopadhyaya B, Di CG, Higashiyama H, Knott GW, Kuhlman SJ, Welker E, Huang ZJ. Experience and activity-dependent maturation of perisomatic GABAergic innervation in primary visual cortex during a postnatal critical period. J Neurosci. 2004; 24:9598–9611. [PubMed: 15509747]

Chen X, Sirois JE, Lei Q, Talley EM, Lynch C III, Bayliss DA. HCN subunit-specific and cAMP-modulated effects of anesthetics on neuronal pacemaker currents. J Neurosci. 2005; 25:5803–5814. [PubMed: 15958747]

Chen L, McKenna JT, Leonard MZ, Yanagawa Y, McCarley RW, Brown RE. GAD67-GFP knock-in mice have normal sleep-wake patterns and sleep homeostasis. Neuroreport. 2010; 21:216–220. [PubMed: 20051926]

Detari L, Rasmusson DD, Semba K. The role of basal forebrain neurons in tonic and phasic activation of the cerebral cortex. Prog Neurobiol. 1999; 58:249–277. [PubMed: 10341363]

Deurveilher S, Lo H, Murphy JA, Burns J, Semba K. Differential c-Fos immunoreactivity in arousal-promoting cell groups following systemic administration of caffeine in rats. J Comp Neurol. 2006; 498:667–689. [PubMed: 16917819]

Duque A, Balatoni B, Detari L, Zaborszky L. EEG correlation of the discharge properties of identified neurons in the basal forebrain. J Neurophysiol. 2000; 84:1627–1635. [PubMed: 10980032]

Endo T, Takazawa K, Kobayashi S, Onaya T. Immunochemical and immunohistochemical localization of parvalbumin in rat nervous tissues. J Neurochem. 1986; 46:892–898. [PubMed: 3512774]

Fisher RS, Buchwald NA, Hull CD, Levine MS. GABAergic basal forebrain neurons project to the neocortex: the localization of glutamic acid decarboxylase and choline acetyltransferase in feline corticopetal neurons. J Comp Neurol. 1988; 272:489–502. [PubMed: 2843581]

Franciosi S, Yanagawa Y, McCarley RW, Brown RE. The putative sleep homeostatic factor adenosine selectively inhibits one type of basal forebrain GABA neurons. Sleep. 2008; 31:A44.

Franklin, KBJ.; Paxinos, G. The mouse brain in stereotaxic coordinates. 3rd. New York: Academic Press; 2008.

Freund TF, Meskenaite V. gamma-Aminobutyric acidcontaining basal forebrain neurons innervate inhibitory interneurons in the neocortex. Proc Natl Acad Sci U S A. 1992; 89:738–7342. [PubMed: 1731348]

Fuller P, Sherman D, Pedersen NP, Saper CB, Lu J. Reassessment of the structural basis of the ascending arousal system. J Comp Neurol. 2011; 519:933–956. [PubMed: 21280045]

Furuta T, Koyano K, Tomioka R, Yanagawa Y, Kaneko T. GABAergic basal forebrain neurons that express receptor for neurokinin B and send axons to the cerebral cortex. J Comp Neurol. 2004; 473:43–58. [PubMed: 15067717]

Galarreta M, Hestrin S. Electrical and chemical synapses among parvalbumin fast-spiking GABAergic interneurons in adult mouse neocortex. Proc Natl Acad Sci U S A. 2002; 99:12438–12443. [PubMed: 12213962]

Gerber U, Greene RW, Haas HL, Stevens DR. Characterization of inhibition mediated by adenosine in the hippocampus of the rat in vitro. J Physiol Lond. 1989; 417:567–578. [PubMed: 2559967]

Gregoriou GG, Gotts SJ, Zhou H, Desimone R. High-frequency, long-range coupling between prefrontal and visual cortex during attention. Science. 2009; 324:1207–1210. [PubMed: 19478185]

Gritti I, Mainville L, Jones BE. Codistribution of GABA-with acetylcholine-synthesizing neurons in the basal forebrain of the rat. J Comp Neurol. 1993; 329:438–457. [PubMed: 8454735]

Gritti I, Mainville L, Jones BE. Projections of GABAergic and cholinergic basal forebrain and GABAergic preoptic-anterior hypothalamic neurons to the posterior lateral hypothalamus of the rat. J Comp Neurol. 1994; 339:251–268. [PubMed: 8300907]

Gritti I, Mainville L, Mancia M, Jones BE. GABAergic and other noncholinergic basal forebrain neurons, together with cholinergic neurons, project to the mesocortex and isocortex in the rat. J Comp Neurol. 1997; 383:163–177. [PubMed: 9182846]

Gritti I, Mariotti M, Mancia M. GABAergic and cholinergic basal forebrain and preoptic-anterior hypothalamic projections to the mediodorsal nucleus of the thalamus in the cat. Neuroscience. 1998; 85:149–178. [PubMed: 9607710]

Gritti I, Manns ID, Mainville L, Jones BE. Parvalbumin, calbindin, or calretinin in cortically projecting and GABAergic, cholinergic, or glutamatergic basal forebrain neurons of the rat. J Comp Neurol. 2003; 458:11–31. [PubMed: 12577320]

Hassani OK, Lee MG, Henny P, Jones BE. Discharge profiles of identified GABAergic in comparison to choliner-gic and putative glutamatergic basal forebrain neurons across the sleep-wake cycle. J Neurosci. 2009; 29:11828–11840. [PubMed: 19776269]

Henny P, Jones BE. Projections from basal forebrain to prefrontal cortex comprise cholinergic, GABAergic and glutamatergic inputs to pyramidal cells or interneurons. Eur J Neurosci. 2008; 27:654–670. [PubMed: 18279318]

Jones BE. Activity, modulation and role of basal forebrain cholinergic neurons innervating the cerebral cortex. Prog Brain Res. 2004; 145:157–169. [PubMed: 14650914]

Jourdain A, Semba K, Fibiger HC. Basal forebrain and mesopontine tegmental projections to the reticular thalamic nucleus: an axonal collateralization and immunohistochemical study in the rat. Brain Res. 1989; 505:55–65. [PubMed: 2575437]

Kalinchuk AV, McCarley RW, Stenberg D, Porkka-Heiskanen T, Basheer R. The role of cholinergic basal forebrain neurons in adenosine-mediated homeostatic control of sleep: lessons from 192 IgG-saporin lesions. Neuroscience. 2008; 157:238–253. [PubMed: 18805464]

Kalogiannis M, Grupke SL, Potter PE, Edwards JG, Chemelli RM, Kisanuki YY, Yanagisawa M, Leonard CS. Narcoleptic orexin receptor knockout mice express enhanced cholinergic properties in laterodorsal tegmental neurons. Eur J Neurosci. 2010; 32:130–142. [PubMed: 20576035]

Kaur S, Junek A, Black MA, Semba K. Effects of ibotenate and 192IgG-saporin lesions of the nucleus basalis magnocellularis/substantia innominata on spontaneous sleep and wake states and on recovery sleep after sleep deprivation in rats. J Neurosci. 2008; 28:491–504. [PubMed: 18184792]

Kim T, McKenna JT, McNally JM, Winston S, Yang C, Chen L, Kocsis B, Deisseroth K, Strecker RE, McCarley RW, Brown RE, Basheer R. Optogenetic stimulation of parvalbumin-positive basal forebrain neurons entrains cortical gamma oscillations and promotes wakefulness. Soc Neurosci Abs. 2011; 286:15.

Kim M, Soontornniyomkij V, Ji B, Zhou X. System-wide immunohistochemical analysis of protein co-localization. PLoS One. 2012; 7:e32043. [PubMed: 22363794]

Levey AI, Armstrong DM, Atweh SF, Terry RD, Wainer BH. Monoclonal antibodies to choline acetyltransferase: production, specificity, and immunohistochemistry. J Neurosci. 1983; 3:1–9. [PubMed: 6822847]

Li Y, Gao XB, Sakurai T, van den Pol AN. Hypocretin/Orexin excites hypocretin neurons via a local glutamate neuron-A potential mechanism for orchestrating the hypo-thalamic arousal system. Neuron. 2002; 36:1169–1181. [PubMed: 12495630]

Lin SC, Nicolelis MA. Neuronal ensemble bursting in the basal forebrain encodes salience irrespective of valence. Neuron. 2008; 59:138–149. [PubMed: 18614035]

Manns ID, Alonso A, Jones BE. Discharge profiles of juxtacellularly labeled and immunohistochemically identified GABAergic basal forebrain neurons recorded in association with the electroencephalogram in anesthetized rats. J Neurosci. 2000; 20:9252–9263. [PubMed: 11125003]

Martin-Ibanez R, Crespo E, Urban N, Sergent-Tanguy S, Herranz C, Jaumot M, Valiente M, Long JE, Pineda JR, Andreu C, Rubenstein JL, Marin O, Georgopoulos K, Mengod G, Farinas I, Bachs O, Alberch J, Canals JM. Ikaros-1 couples cell cycle arrest of late striatal precursors with neurogenesis of enkephalinergic neurons. J Comp Neurol. 2010; 518:329–351. [PubMed: 19950118]

McCurry CL, Shepherd JD, Tropea D, Wang KH, Bear MF, Sur M. Loss of Arc renders the visual cortex impervious to the effects of sensory experience or deprivation. Nat Neurosci. 2010; 13:450–457. [PubMed: 20228806]

McDonald AJ, Muller JF, Mascagni F. Postsynaptic targets of GABAergic basal forebrain projections to the basolateral amygdala. Neuroscience. 2011; 183:144–159. [PubMed: 21435381]

McKenna JT, Rigby MS, Chen L, Winston S, Yanagawa Y, McCarley RW, Brown RE. GAD67-GFP knock-in mice as a tool to investigate GABAergic neurons involved in behavioral state control. Sleep. 2010; 33:A136.

McKenna JT, Abarr KK, Rigby MS, Yanagawa Y, McCarley RW, Brown RE. Distribution and interaction between cortically projecting basal forebrain neurons investigated using mutant mouse strains expressing fluorescent proteins in GABAergic and parvalbumin. Sleep. 2011; 34:A85.

McNally JM, McCarley RW, McKenna JT, Yanagawa Y, Brown RE. Complex receptor mediation of acute ketamine application on in vitro gamma oscillations in mouse prefrontal cortex: modeling gamma band oscillation abnormalities in schizophrenia. Neuroscience. 2011; 199:51–63. [PubMed: 22027237]

Morris NP, Harris SJ, Henderson Z. Parvalbumin-immunoreactive, fast-spiking neurons in the medial septum/diagonal band complex of the rat: intracellular recordings in vitro. Neuroscience. 1999; 92:589–600. [PubMed: 10408608]

Oliva AA Jr, Jiang M, Lam T, Smith KL, Swann JW. Novel hippocampal interneuronal subtypes identified using transgenic mice that express green fluorescent protein in GABAergic interneurons. J Neurosci. 2000; 20:3354–3368. [PubMed: 10777798]

Onteniente B, Tago H, Kimura H, Maeda T. Distribution of gamma-aminobutyric acid-immunoreactive neurons in the septal region of the rat brain. J Comp Neurol. 1986; 248:422–430. [PubMed: 3522664]

Ottersen OP, Storm-Mathisen J. Glutamate- and GABA-containing neurons in the mouse and rat brain, as demonstrated with a new immunocytochemical technique. J Comp Neurol. 1984; 229:374–392. [PubMed: 6150049]

Panula P, Revuelta AV, Cheney DL, Wu JY, Costa E. An immunohistochemical study on the location of GABAergic neurons in rat septum. J Comp Neurol. 1984; 222:69–80. [PubMed: 6365983]

Peng Z, Houser CR. Temporal patterns of fos expression in the dentate gyrus after spontaneous seizures in a mouse model of temporal lobe epilepsy. J Neurosci. 2005; 25:7210–7220. [PubMed: 16079403]

Perrotti LI, Hadeishi Y, Ulery PG, Barrot M, Monteggia L, Duman RS, Nestler EJ. Induction of deltaFosB in reward-related brain structures after chronic stress. J Neurosci. 2004; 24:10594–105602. [PubMed: 15564575]

Pinault D, Deschenes M. Control of 40-Hz firing of reticular thalamic cells by neurotransmitters. Neuroscience. 1992; 51:259–268. [PubMed: 1361219]

Rye DB, Wainer BH, Mesulam MM, Mufson EJ, Saper CB. Cortical projections arising from the basal forebrain: a study of cholinergic and noncholinergic components employing combined retrograde tracing and immunohistochemical localization of choline acetyltransferase. Neuroscience. 1984; 13:627–643. [PubMed: 6527769]

Rye DB, Saper CB, Lee HJ, Wainer BH. Pedunculopontine tegmental nucleus of the rat: cytoarchitecture, cytochemistry, and some extrapyramidal connections of the mesopontine tegmentum. J Comp Neurol. 1987; 259:483–528. [PubMed: 2885347]

Semba K, Fibiger HC. Afferent connections of the laterodorsal and the pedunculopontine tegmental nuclei in the rat: a retro- and antero-grade transport and immunohistochemical study. J Comp Neurol. 1992; 323:387–410. [PubMed: 1281170]

Seto-Ohshima A, Aoki E, Semba R, Emson PC, Heizmann CW. Appearance of parvalbumin-specific immunoreactivity in the cerebral cortex and hippocampus of the developing rat and gerbil brain. Histochemistry. 1990; 94:579–589. [PubMed: 2279955]

Siembab VC, Smith CA, Zagoraiou L, Berrocal MC, Mentis GZ, Alvarez FJ. Target selection of proprioceptive and motor axon synapses on neonatal V1-derived Ia inhibitory interneurons and Renshaw cells. J Comp Neurol. 2010; 518:4675–46701. [PubMed: 20963823]

Smith ML, Hale BD, Booze RM. Calbindin-D28k immunoreactivity within the cholinergic and GABAergic projection neurons of the basal forebrain. Exp Neurol. 1994; 130:230–236. [PubMed: 7867752]

Sohal VS, Zhang F, Yizhar O, Deisseroth K. Parvalbumin neurons and gamma rhythms enhance cortical circuit performance. Nature. 2009; 459:698–702. [PubMed: 19396159]

Solbach S, Celio MR. Ontogeny of the calcium binding protein parvalbumin in the rat nervous system. Anat Embryol (Berl). 1991; 184:103–124. [PubMed: 1952098]

Spreafico R, Battaglia G, Frassoni C. The reticular thalamic nucleus (RTN) of the rat: cytoarchitectural, Golgi, immunocytochemical, and horseradish peroxidase study. J Comp Neurol. 1991; 304:478–490. [PubMed: 1708789]

Stillman AA, Krsnik Z, Sun J, Rasin MR, State MW, Sestan N, Louvi A. Developmentally regulated and evolutionarily conserved expression of SLITRK1 in brain circuits implicated in Tourette syndrome. J Comp Neurol. 2009; 513:21–37. [PubMed: 19105198]

Strecker RE, Morairty S, Thakkar MM, Porkka-Heiskanen T, Basheer R, Dauphin LJ, Rainnie DG, Portas CM, Greene RW, McCarley RW. Adenosinergic modulation of basal forebrain and

preoptic/anterior hypothalamic neuronal activity in the control of behavioral state. Behav Brain Res. 2000; 115:183–204. [PubMed: 11000420]

Suzuki N, Bekkers JM. Inhibitory neurons in the anterior piriform cortex of the mouse: classification using molecular markers. J Comp Neurol. 2010; 518:1670–1687. [PubMed: 20235162]

Tamamaki N, Yanagawa Y, Tomioka R, Miyazaki J, Obata K, Kaneko T. Green fluorescent protein expression and colocalization with calretinin, parvalbumin, and somatostatin in the GAD67-GFP knock-in mouse. J Comp Neurol. 2003; 467:60–79. [PubMed: 14574680]

Tiesinga P, Sejnowski TJ. Cortical enlightenment: are attentional gamma oscillations driven by ING or PING? Neuron. 2009; 63:727–732. [PubMed: 19778503]

Unal CT, Golowasch JP, Zaborszky L. Adult mouse basal forebrain harbors two distinct cholinergic populations defined by their electrophysiology. Front Behav Neurosci. 2012; 6:21. [PubMed: 22586380]

Varga V, Hangya B, Kranitz K, Ludanyi A, Zemankovics R, Katona I, Shigemoto R, Freund TF, Borhegyi Z. The presence of pacemaker HCN channels identifies theta rhythmic GABAergic neurons in the medial septum. J Physiol. 2008; 586:3893–3915. [PubMed: 18565991]

Xu X, Roby KD, Callaway EM. Mouse cortical inhibitory neuron type that coexpresses somatostatin and calretinin. J Comp Neurol. 2006; 499:144–160. [PubMed: 16958092]

Xu X, Roby KD, Callaway EM. Immunochemical characterization of inhibitory mouse cortical neurons: three chemically distinct classes of inhibitory cells. J Comp Neurol. 2010; 518:389–404. [PubMed: 19950390]

Yang C, Yanagawa Y, McCarley RW, Brown RE. Acetylcholine directly and indirectly increases the excitability of parvalbumin-positive GABAergic neurons in mouse basal forebrain. Sleep. 2011; 34:A90.

Zaborszky L, Carlsen J, Brashear HR, Heimer L. Cholinergic and GABAergic afferents to the olfactory bulb in the rat with special emphasis on the projection neurons in the nucleus of the horizontal limb of the diagonal band. J Comp Neurol. 1986a; 243:488–509. [PubMed: 3512629]

Zaborszky L, Heimer L, Eckenstein F, Leranth C. GABAergic input to cholinergic forebrain neurons: an ultrastructural study using retrograde tracing of HRP and double immunolabeling. J Comp Neurol. 1986b; 250:282–295. [PubMed: 3528237]

Zhao S, Ting JT, Atallah HE, Qiu L, Tan J, Gloss B, Augustine GJ, Deisseroth K, Luo M, Graybiel AM, Feng G. Cell type-specific channelrhodopsin-2 transgenic mice for optogenetic dissection of neural circuitry function. Nat Methods. 2011; 8:745–752. [PubMed: 21985008]

Abbreviations

3V	Third Ventricle
Aca	Anterior commissure, anterior aspect
Acb	Accumbens nucleus
Acp	Anterior commissure, posterior aspect
AMCA	Aminomethylcoumarin acetate
AP	Action potential
BF	Basal forebrain
Cg1	Cingulate cortex, area 1
ChAT	Choline acetyltransferase
Cl	Claustrum
CPu	Caudate putamen
CTX	Cortex
DP	Dorsal peduncular cortex

Fmi	Forceps minor of the corpus callosum
GABA	Gamma-aminobutyric acid
GAD67	Glutamate decarboxylase, 67kD isoform
GFP	Green fluorescent protein
HDB	Horizontal limb of the diagonal band
I_h	Hyperpolarization activated current
IHC	Immunohistochemistry
IL	Infralimbic cortex
IR-DIC	Infrared differential contrast
LPO	Lateral preoptic nucleus
LV	Lateral ventricle
M1	Primary motor cortex
M2	Secondary motor cortex
MCPO	Magnocellular preoptic nucleus
MPA	Medial preoptic area
PFC	Prefrontal cortex
PrL	Prelimbic cortex
PV	Parvalbumin
R_{in}	Input resistance
RLM	Rhodamine latex microspheres
RMP	Resting membrane potential
sEPSPs	Spontaneous excitatory postsynaptic potentials
Tu	Olfactory tubercle
SI	Substantia innominata
VP	Ventral pallidum

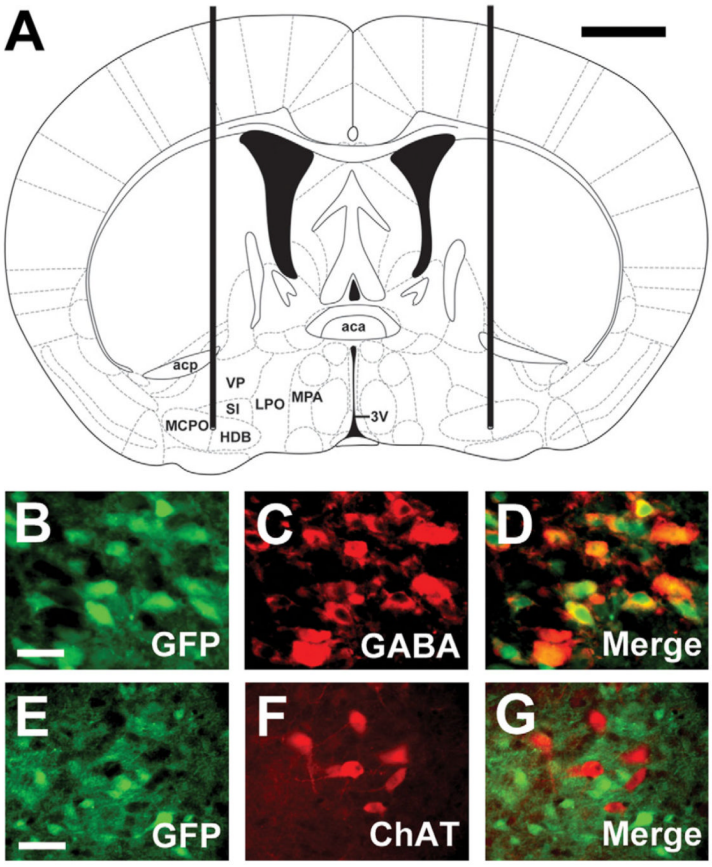

Figure 1.

GFP selectively labels GABAergic neurons in GAD67-GFP knock-in mice. **A**: Schematic illustrating the location of the basal forebrain (BF) and the bilateral cannulae used to inject colchicine (1 μl) into the BF adapted with permission from Franklin and Paxinos, 2008, ©Elsevier). Colchicine pretreatment was used to enhance GABA immunolabeling of cell bodies by inhibition of axonal transport and consequent sequestration of GABA in neuronal cell bodies. 3V, third ventricle; aca, anterior commissure, anterior aspect; acp, anterior commissure, posterior aspect; HDB, horizontal limb of the diagonal band; LPO, lateral preoptic nucleus; MCPO, magnocellular preoptic nucleus; MPA, medial preoptic area; SI, substantia innominata; VP, ventral pallidum. **B**–**D**: Photographic depiction of GFP+ neurons (B, green) colabeled for GABA (C, red) in BF (substantia innominata represented here). Approximately 88% of GFP+ neurons were labeled with GABA in the BF of GAD67-GFP mice (D, yellow/orange neurons in “Merge” overlay). **E**–**G**: GFP (E, green) does not label neighboring cholinergic neurons (G, Merge), stained for choline acetyltransferase (F, ChAT, red). Scale bars = 1 mm in A; 20 μm in B–D; 25 μm in E– G. A magenta-green version for the assistance of color-blind readers is presented as Supporting Figure 1 online.

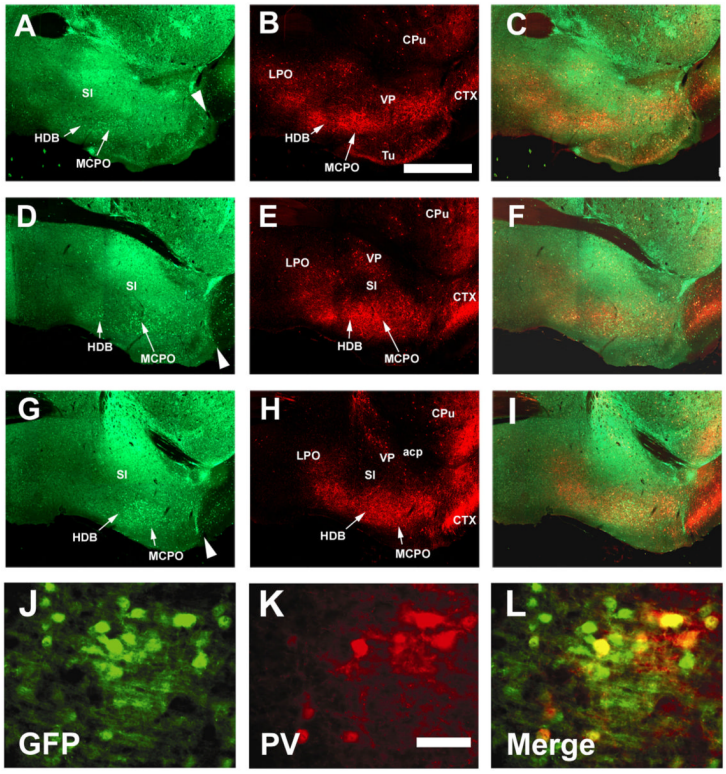

Figure 2.

Fluorescent images of GABAergic (GFP+) and parvalbumin (PV+) neurons in the BF of GAD67-GFP knock-in mice. A–I: Photographic images of GFP+ (**A,D,G**; green), PV+ stained (**B,E,H**; red), and GFP+/PV+ (**C,F,I**; yellow/orange neurons in "Merge" overlay) neuronal perikarya in rostral, medial, and caudal regions of the BF. GFP+ and PV+ fibers are located throughout the BF. Arrowheads indicate the large drop-off in GFP-fiber density at the border of the BF and cortex. A similar but less pronounced drop-off occurs at the medial border of the BF with the preoptic area. CPu, caudate putamen; CTX, cortex; HDB, horizontal limb of the diagonal band; LPO, lateral preoptic nucleus; MCPO, magnocellular preoptic nucleus; SI, substantia innominata; VP, ventral pallidum. **J–L**: PV (K, red) is colocalized in a subset of GABAergic (J, green GFP+) neurons in the BF (L, Merge). Scale bars = 0.5 mm in A–I; 25 lm in J–L. A magenta-green version for the assistance of color-blind readers is presented as Supporting Figure 2 online.

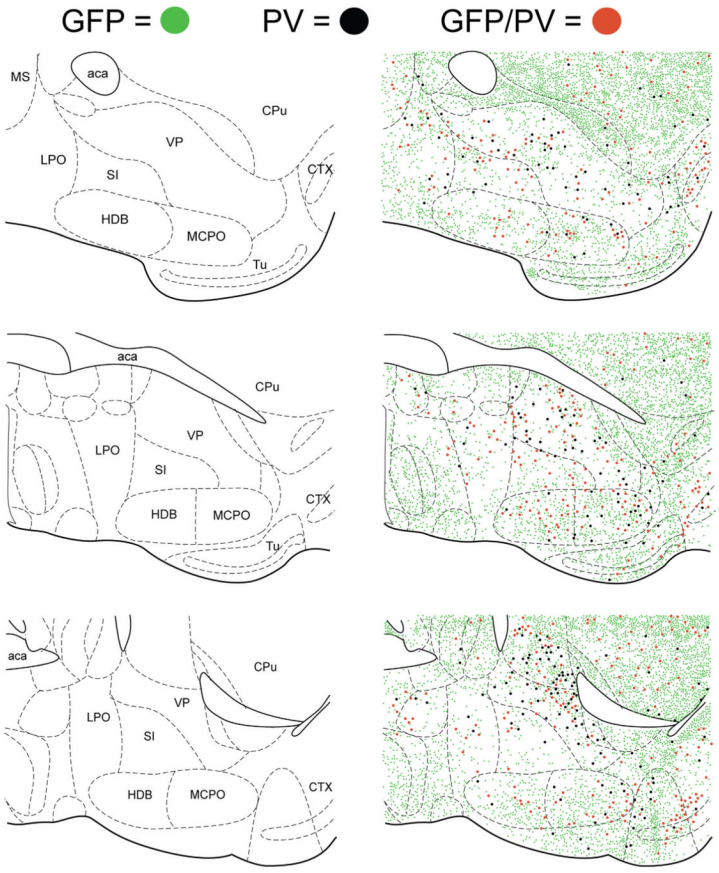

Figure 3.

Mapping of the location of GABAergic (GFP+), parvalbumin (PV+), and GFP+/PV+ neurons in the BF of GAD67-GFP knock-in mice. Schematic representation of GFP+ (green), PV+ (black), and GFP+/PV+ (red) neuronal perikarya in BF plotted on atlas sections (adapted with permission from Franklin and Paxinos, 2008, ©Elsevier). Top: rostral representation = +0.38 mm from bregma; Middle: medial representation = +0.14 mm from bregma; and Bottom: caudal representation = −0.10 mm from bregma. GFP+ neurons were evident throughout BF, and densely concentrated in a central band from the medial horizontal limb of the diagonal band (HDB) and lateral aspect of the magnocellular preoptic area (MCPO), as well as in the olfactory tubercle (Tu). Large numbers of GFP+ neurons were also located in the preoptic area and caudate putamen. PV+ neurons were prominent in VP, HDB, and MCPO regions.

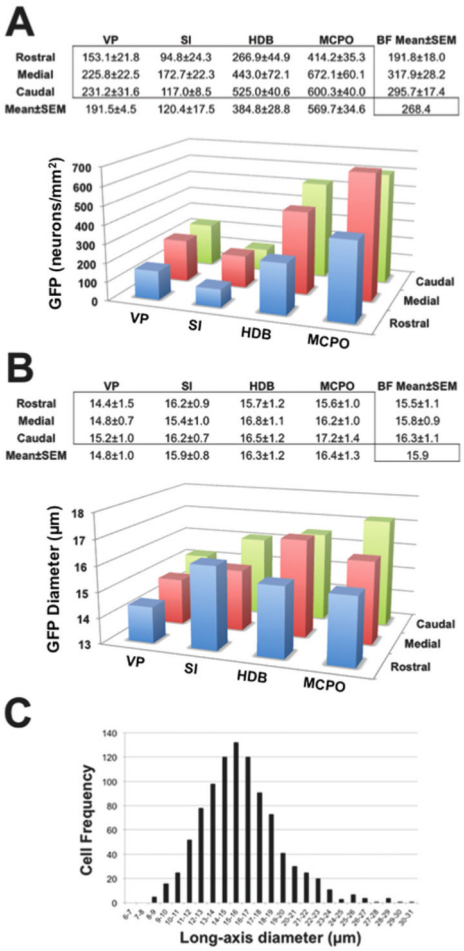

Figure 4.

The density and size of GABAergic (GFP+) neurons in the BF of GAD67-GFP knock-in mice. The density (**A**) and long-axis diameter (**B**) of GFP+ neurons was determined in the ventral pallidum (VP), substantia innominata (SI), horizontal limb of the diagonal band (HDB), and magnocellular preoptic (MCPO) regions of representative rostral, medial, and caudal BF slices. A: The relative density of GFP+ neurons was highest in the magnocellular preoptic area (MCPO), followed by the horizontal limb of the diagonal band (HDB) in the BF of GAD67-GFP mice. Substantially lower densities were found in the substantia innominata (SI) and ventral pallidum (VP). B: No significant differences were found between mean long-axis diameters of different subnuclei or along the rostral-caudal axis. **C**: Histogram illustrating the cell frequency distribution for the long-axis diameters of GABAergic neurons (out of 960 neurons evaluated), centered around a mean of 15.9 μm.

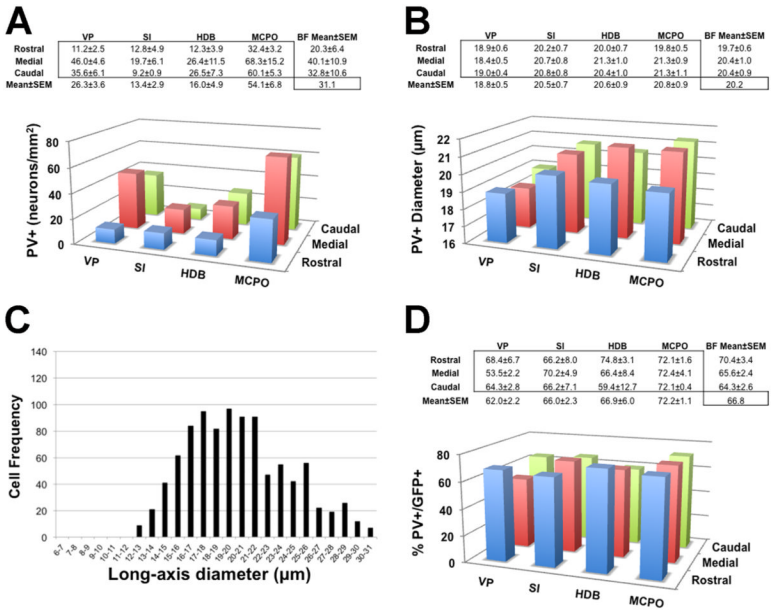

Figure 5.

The density, size, and GFP colocalization of parvalbumin (PV+) neurons in the BF of GAD67-GFP knock-in mice. The density (**A**), long-axis diameter (**B,C**), and extent of GFP colocalization (**D**) of PV+ neurons was determined in the ventral pallidum (VP), substantia innominata (SI), horizontal limb of the diagonal band (HDB), and magnocellular preoptic (MCPO) regions of representative rostral, medial, and caudal BF slices. A: The relative density of PV+ neurons was highest in the magnocellular preoptic area (MCPO), followed by the ventral pallidum. B: PV+ neurons had lower long-axis diameters in VP when compared to SI, HDB or MCPO. C: Histogram illustrating the cel frequency distribution for the long-axis diameters of PV+ neurons (out of 960 neurons evaluated), centered around a mean of 20.2 μm. D: A high percentage (~66%) of PV+ neurons were also GABAergic (GFP+).

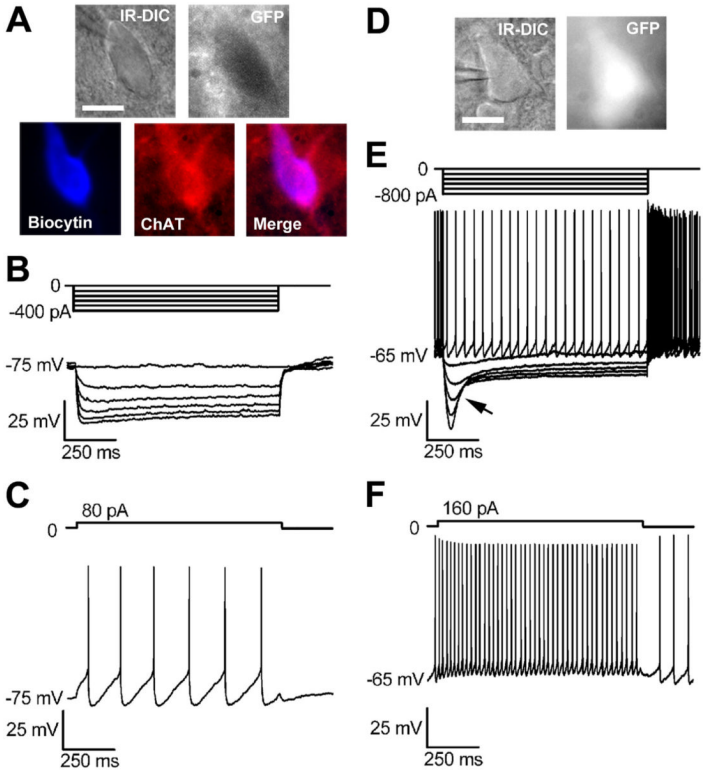

Figure 6.

Distinct intrinsic membrane properties of identified basal forebrain cholinergic and large-sized (>20 μm) GABAergic neurons. **A**–**C**: Cholinergic (GFP-Negative, ChAT+) neurons are slow firing neurons with large afterhyperpolarizations. **A**: Top: Black and white infrared differential contrast (IR-DIC, left) and fluorescent images of the recorded neuron in the slice. This neuron has a lower green fluorescent protein (GFP, right) fluorescence than the background neuropil, i.e., it is GFP-negative. Bottom: Post-hoc labeling following fixation of the slice in 10% formalin. The recorded neuron was labeled for biocytin (AMCA, blue, left) contained in the intracellular patch solution and was positive for choline acetyltransferase (ChAT-A594, red, middle), the synthetic enzyme for acetylcholine, i.e., it was a cholinergic neuron (Merge, right). **B**: Response to no current or hyperpolarizing current steps. The size of the steps was titrated according to the input resistance of the recorded neuron (see methods). This cell was silent (no action potentials in the absence of current injection. **C**: When depolarized this neuron fired slowly and had large afterhyperpolarizations. **D**–**F**: Large GABAergic (GFP+) neurons are spontaneously active, fast-firing neurons with a prominent depolarizing sag during current pulses (arrow in E). D: Black and white infrared differential contrast (IR-DIC, left) and fluorescent images of the recorded neuron in the slice. This neuron has a higher green fluorescent protein (GFP, right) fluorescence than the background neuropil, i.e., it is GFP+ (GABAergic). E: Response to no current or hyperpolarizing current steps. The size of the steps was titrated according to the input resistance of the recorded neuron (see methods). This cell was spontaneously active (fired action potentials in the absence of current injection). Hyperpolarizing current steps revealed a prominent depolarizing sag during the step. F: When depolarized this neuron fired very rapidly with small afterhyperpolarizations.

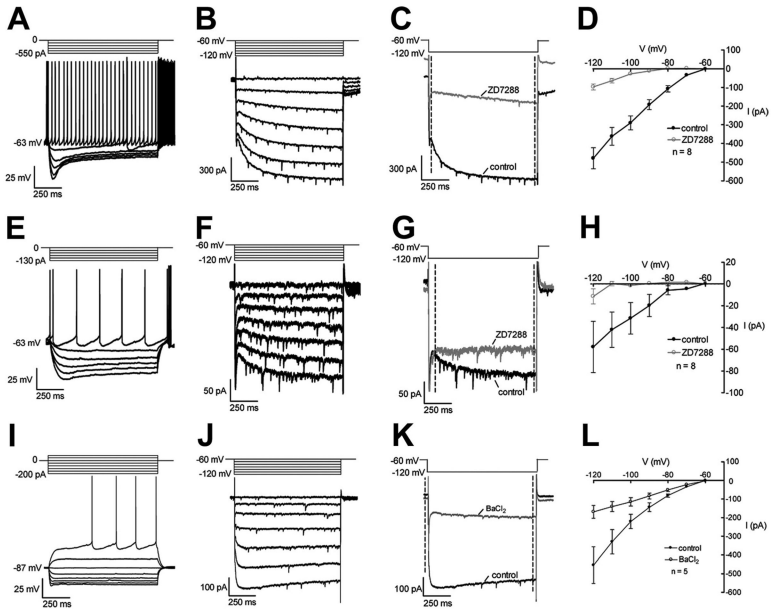

Figure 7.

BF GABAergic (GFP+) neurons can be subdivided into three groups based on their intrinsic membrane properties. The first group (**A**–**D**) consists of neurons with a large depolarizing sag with a biexponential decay during hyperpolarizing current pulses (A) and arge inward (H)-currents in voltage-clamp (B) which are blocked (C,D) by the specific pharmacological inhibitor, ZD7288 (100 μM). These neurons have a depolarizing resting membrane potential and fire spontaneously at high rates in the absence of injected current. The second group (**E**–**H**) consists of neurons with a smaller depolarizing sag with a monoexponential decay during hyperpolarizing current pulses (E) and smaller inward (H)-currents in voltage-clamp (F) which are blocked (G,H) by ZD7288 (100 μM). These neurons also have a depolarizing resting membrane potential and fire spontaneously at high rates in the absence of injected current. The third group (**I**–**L**) is silent at rest and exhibits a time-independent rectification during hyperpolarizing pulses which is blocked by the inward rectifying potassium channel inhibitor, barium chloride (100 μm). A,E,I: Voltage responses of different types of neurons to current steps of 1-second duration in current-clamp. The size of the steps was titrated to compensate for differences in input resistance (see Materials and Methods). Large I_h and small I_h neurons fired spontaneously in the absence of injected current. The third type of neuron was silent at rest and required depolarizing steps to elicit action potentials (I). B,F,J: Current responses to hyperpolarizing current steps of 1 s duration in voltage-clamp (V_h = −60 mV). All three types of neurons exhibit inward rectification but for the first two types, this rectification is time-dependent and blocked by the H-current blocker (ZD7288, 100 μM, C,G), whereas the third type demonstrates instantaneous rectification blocked by the inhibitor of inwardly rectifying potassium currents, $BaCl_2$ (100 μM, K). D,H,L: Mean data for the block of time-dependent rectification by ZD7288 (D,H) and instantaneous rectification by $BaCl_2$ (L). The current plotted on the y-axis represents a subtraction of the baseline current from the current induced by the voltage step (indicated by the dotted lines in C,G,K).

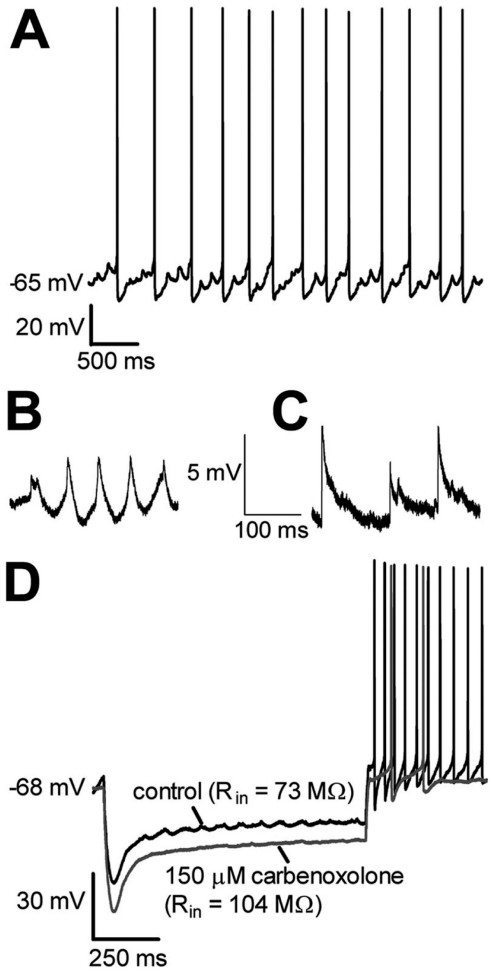

Figure 8.

A subset of large BF GABAergic neurons exhibits “spi-kelets” which are blocked by the gap junction blocker, carbenoxolone. **A**: Subthreshold oscillations (spikelets) are evident in the interspike interval. **B**: Spikelets have a slow rising phase and a slow decay phase. **C**: Spontaneous excitatory postsynaptic potentials (sEPSPs, blocked by a cocktail of the glutamatergic receptor antagonists DNQX [5 μM] and D-AP5 [50 μM]) have a distinctly different time course, with a very fast rising phase and a much slower decay phase. **D**: Carbenoxolone blocks spikelets and increases input resistance. Current step: −750 pA, 1 second.

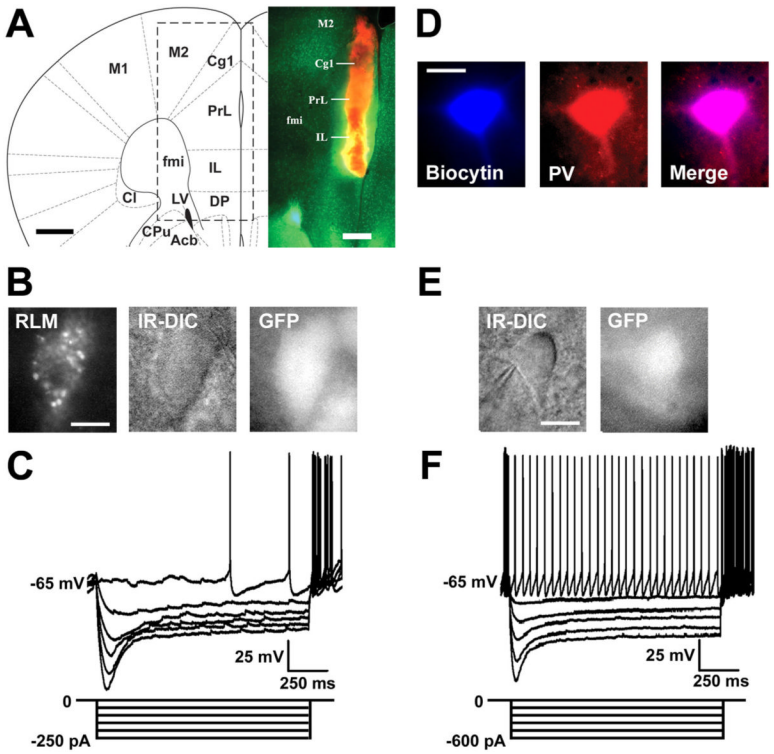

Figure 9.

GABAergic BF neurons retrogradely labeled from the prefrontal cortex (**A**–**C**) and those identified post-hoc by immunohistochemis-try as parvalbumin-positive (**D**–**F**) have similar properties. Both GABAergic neurons retrogradely labeled from the cortex and those which are PV+ are spontaneously active and have prominent depolarizing sags during hyperpolarizing current steps. A: Injection site of rhodamine latex microspheres (RLM, red) in the prefrontal cortex of GAD67-GFP mice. Left: Schematic showing the location of the injection (adapted with permission from Franklin and Paxinos, 2008, ©Elsevier). The dotted box indicates the region shown on the right. Right: Fluorescence image showing the injection site. Acb, accumbens nucleus; Cg1, cingulate cortex, area 1; Cl, claustrum; CPu, caudate putamen; DP, dorsal peduncular nucleus; fmi, forceps minor of the corpus callosum; IL, infralimbic cortex; LV, lateral ventricle; M1, primary motor cortex; M2, secondary motor cortex; PrL, prelimbic cortex. B: Black-and-white images of the recorded neuron. Left: Fluorescence image of the punctate labeling of the rhodamine latex microspheres under the rhodamine filter set, confirming retrograde labeling from the prefrontal cortex; Middle: Infrared differential contrast (IR-DIC) image; Right: Fluorescent images of the same cell using the green fluorescence protein filter. C: Spontaneous firing and response to hyperpolarizing current pulses of a retrogradely labeled BF GABAergic neuron. D: Post-hoc labeling following fixation of the slice in 10% formalin. The recorded neuron was labeled for biocytin (AMCA, blue, left) contained in the intracellular patch solution and was PV+ (PV-A594, red, middle). **E**: Black-and-white images of the recorded neuron. Left: Infrared differential contrast (IR-DIC) image; Right: Fluorescent images of the same cell using the green fluorescence protein filter. **F**: Spontaneous firing and response to hyperpolarizing current pulses of a post-hoc labeled BF GABA/PV+ neuron. Scale bars = 0.5 mm in B, D, and E.

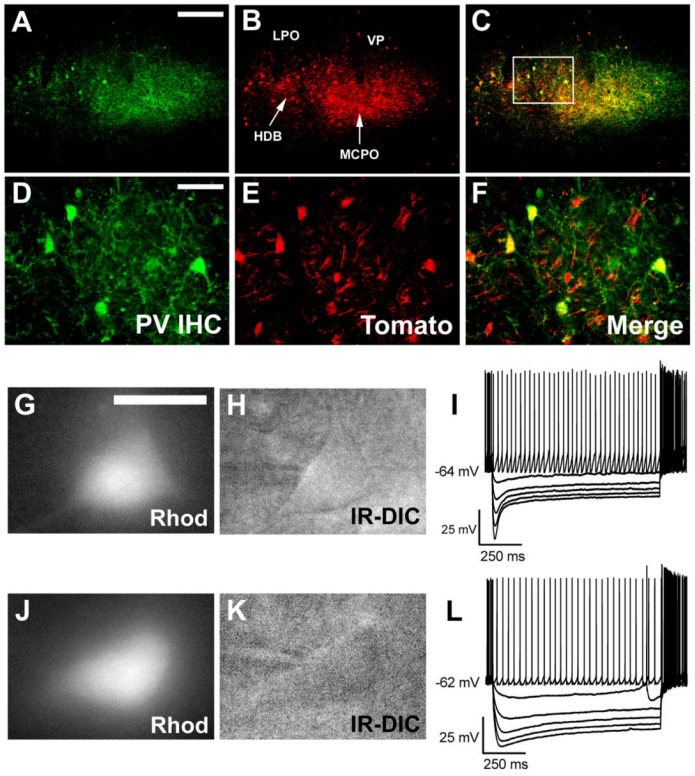

Figure 10.

Intrinsic membrane properties of parvalbumin-positive (PV+) neurons in the BF of PV-Tomato mice. A: Colocalization of endogenous PV+ red fluorescent neurons with a PV antibody in the PV-Tomato mouse: **A,D**: Fluorescent images of PV+ neurons (green), labeled by means of immunohistochemistry (IHC). **B,E**: fluorescent images of PV-Tomato (red) neurons. HDB, horizontal limb of the diagonal band; LPO, lateral preoptic area; MCPO, magnocellular preoptic area; VP, ventral pallidum. **C,F**: overlay of green and red fluorescent images (Merge). Orange/yellow neurons indicate signal colocalization. **G**–**L**: Intrinsic membrane properties of PV+ neurons in the BF of PV-Tomato mice. PV+ neurons fire spontaneously at high rates and have prominent depolarizing sags during hyperpolarizing current pulses. As with arge GFP+ neurons in GAD67-GFP knock-in mice, the PV+ neurons could be subdivided into two subgroups (G-I: Large sag, biexponentia decay; J–L: Smaller sag, monoexponential decay) based on the size and kinetics of the depolarizing sag. Black-and-white images of the recorded neuron when using the rhodamine filter illumination (G,J; Rhod) or under infrared differential contrast (H,K; IR-DIC). I,L: Spontaneous firing and response to hyperpolarizing current pulses of PV+ neurons in the BF of PV-Tomato mice. Current step size: −200 pA, (I), −170 pA (L). Scale bars = Low Mag, 100 μm; High Mag, 25 μm in A–F; 25 μm in G,H,J,K. A magenta-green version for the assistance of color-blind readers is presented as Supporting Figure 3 online.

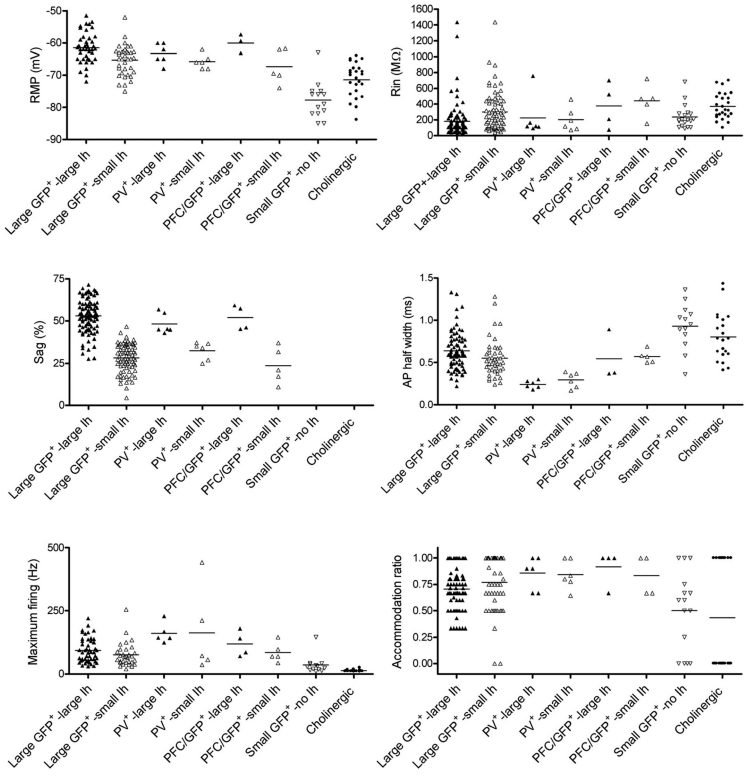

Figure 11.

Scatterplots of the intrinsic membrane properties of the neurons recorded in this study. The resting membrane potential (RMP), input resistance (Rin), depolarizing sag, action potential (AP) half width, maximal tonic firing rate, and accommodation ratio (number of action potentials in the last 100 ms of a 1-second depolarizing step/number of action potentials during the first 100 ms) of green fluorescent protein positive (GFP+), parvalbumin positive (PV+), and GFP+ neurons labeled from the prefrontal cortex (PFC) are compared to those of cholinergic neurons. GFP+ and PV+ neurons are subdivided into large I_h and small I_h subgroups based on the kinetics of the depolarizing sag (see Results).

Table 1

Antibody Characterization

Antigen	Validation	Host species	Source/cat. no.	Dilution	References
Gamma-aminobutyric acid (GABA)	Synthetic GABA conjugates to bovine albumin serum (BSA), binding to GABA but not BSA (dot blot assays)	Rabbit	Sigma (St. Louis, MO) A2052	1:200	(Suzuki and Bekkers, 2010) (Xu et al., 2010) (Stillman et al., 2009)
Choline acetyltransferase (ChAT)	68-kDa band on western blots from human placental cells	Rabbit	Millipore (Billerica, MA) AB143	1:200	(Martin-Ibanez et al., 2010) (Hassani et al., 2009) (Stillman et al., 2009)
Parvalbumin(PV, Abcam)	12-kDa band on western blot assays Purified from rat muscle	Rabbit	Abcam (Cambridge, MA) AB11427	1:200	(Akgul and Wollmuth, 2010) (McCurry et al., 2010) (Bowser and Khakh, 2004)
Parvalbumin (PV, Millipore)	12-kDa band on western blot assays Purified from frog muscle	Mouse	Millipore (Billerica, MA) MAB1572	1:200	(Siembab et al., 2010) (Peng and Houser, 2005) (Perrotti et al., 2004)

Table 2

Summary of the Intrinsic Membrane Properties of BF Neurons

	Large (> 20 μm) GFP+ neurons in (GAD67-GFP mice)			PV+ neurons (PV-Tomato mice)		Retrogradely labeled from PFC/ GFP+ (GAD67-GFP mice)		Small GFP+ (< 20 lm) (GAD67-GFP mice)	Cholinergic (GFP-Neg)
Neuronal type	**All (n=166)**	**Large Ih (n=89)**	**Small Ih (n=77)**	**Large Ih (n=6)**	**Small Ih (n=6)**	**Large Ih (n=4)**	**Small Ih (n=5)**	**No Ih (n=19)**	**N=26 (ChAT+n=13)**
Long diameter (μm)	24.4±0.4	24.3±0.5	24.5±0.8	24.0±1.1	24.8±1.1	18.0 ± 2.5	20.6±1.9	**14.2±0.5**	24.4±0.8
Short diameter (μm)	13.7±0.2	13.9±0.3	13.6±0.3	17.7±1.6	17. ±1.8	11.8 ± 2.6	10.6±0.7	9.7±0.5	15.9±0.7
RMP (mV)	**−63.3±0.6**	−61.5±0.7	−65.4±0.8	−63.0±1.3	−66±0.9	−60.0±1.7	−67.4±2.5	**−77.7±1.5**	**−71.5±1.0**
Rin (MΩ)	236±18	181 ±23	300±28	227±106	203±61	377±143	441 ±91	300±28	370±32
Sag %	**41.4±1.2**	**52.9±1.1**	**28.1±1.0**	**51.8 ± 2.4**	**32.4±2.2**	**52.0±3.7**	**24.5±4.8**	-	-
Sag decay τ (ms)	-	**53.1 ±0.8 (Fast)**	**472±191**	**42.0±4.7 (Fast)**	**200±27**	**45.1 ±4.8 (Fast)**	**218±52**	-	-
		574±90 (Slow)		**464±83 (Slow)**		**533 ± 133 (Slow)**			
Spontaneous firing (Hz)	**12.9±0.8**	15.0±1.2	10.3±1.1 (n=64/77)	15.6±6.6	21.2±5.0	12.7±4.7	8.5±2.2	**0**	1.1 ±0.5 (n =11/26)
Maximum firing (Hz)	87±5	94±7	76±9	**162±18**	**164±76**	120±25	85±17	**36±10**	**13.7±0.8**
AP half width (ms)	0.61 ±0.02	0.64±0.03	0.56±0.03	**0.27±0.02**	**0.30±0.04**	0.55±0.17	0.57±0.03	0.92±0.07	0.80±0.06
AP threshold (mV)	−53.8± 1.1	−52.6±2.0	−55.4 ±0.4	−52.8±2.6	−56.9±0.7	−57.6±0.8	−52.3±1.8	−56.1 ±0.8	−52.1 ±0.5
AP amplitude (mV)	76.1 ±0.9	76.5±1.0	75.7 ± 1.6	67.3±4.1	69.8±4.0	88.3±3.8	69.8±3.6	74.0±1.7	74.4±1.2
AHP(mV)	**−15.3±0.3**	−14.3±0.4	−16.6± 0.5	−18.7±2.1	−15.2±2.1	−21.4±3.4	−17.9±0.7	**−8.4±1.0**	**−26.4±1.0**

Data are presented as mean ± SEM. Figures in bold represent characteristics that define the neuronal class. AHP, afterhyperpolarization; AP, action potential; GFP, green fluorescent protein; Ih, hyperpolariza-tion activated cation current (causing a depolarizing sag in current-clamp); PV, parvalbumin; Rin, input resistance; RMP, resting membrane potential; τ, exponential time constant for the decay of the depolarizing sag during hyperpolarizing pulses to −110 mV.